

# D4C Glove-train: Solving the RPM and Bongard-logo Problem by Circumscribing and Building Distribution for Concepts

Ruizhuo Song, Member, IEEE, Beiming Yuan

**Abstract**—This paper achieves noteworthy progress in the realm of abstract reasoning, particularly in addressing Raven’s Progressive Matrices (RPM) and Bongard-Logo challenges. Initially, we introduce Lico-Net, a novel baseline model that resolves RPM problems with remarkable accuracy. Leveraging this foundation, we advance with the D3C approach, which advocates representing the underlying concepts in abstract reasoning problems through distributions. This perspective enhances the performance of both Lico-Net and a baseline model excelling in Bongard-Logo tasks. To bolster the computational efficiency of D3C, we present the D3C-cos variant, offering a streamlined solution. Furthermore, we propose the D2C method, redefining concept boundaries within these domains and bridging the divide between high-level abstractions and their lower-dimensional counterparts. Finally, we extend our methodology to D4C, employing adversarial techniques to refine concept boundaries further and demonstrate substantial improvements in both RPM and Bongard-Logo challenges. Overall, our contributions present a fresh outlook and practical advancements in the field of abstract reasoning.

**Index Terms**—Abstract reasoning, Raven’s Progressive Matrices, Bongard-logo problem, Adversarial Learning.

## I. INTRODUCTION

DEEP neural networks have achieved remarkable success in various domains, including computer vision [1]–[3], natural language processing [4]–[6], generative models [7]–[9], visual question answering [10], [11], and abstract reasoning [12]–[14]. This success is primarily attributed to the remarkable capabilities of deep learning, which can recognize text, images, and sound data by learning the inherent patterns and representational hierarchies within sample data, thereby demonstrating analytical learning abilities similar to humans. Especially when addressing complex pattern recognition problems, the powerful capabilities of deep learning enable it to mimic human activities, further advancing the progress of artificial intelligence-related technologies. Its outstanding performance in speech and image recognition has surpassed previous technologies in terms of recognition accuracy.

This work was supported by the National Natural Science Foundation of China under Grants 62273036. Corresponding author: Ruizhuo Song, ruizhuosong@ustb.edu.cn

Ruizhuo Song and Beiming Yuan are with the Beijing Engineering Research Center of Industrial Spectrum Imaging, School of Automation and Electrical Engineering, University of Science and Technology Beijing, Beijing 100083, China (Ruizhuo Song email: ruizhuosong@ustb.edu.cn and Beiming Yuan email: d202310354@xs.ustb.edu.cn).

Ruizhuo Song and Beiming Yuan contributed equally to this work.

However, despite these impressive accomplishments in deep learning, there are still a series of unresolved issues and challenges that require further research and exploration. For instance, research is ongoing on how to utilize the results of upperlayer training as initialization parameters for lowerlayer training, aiming to enhance the efficiency of deep model training. Additionally, layer-wise initialization training with unsupervised learning constitutes a significant strategy within the field of deep learning.

Especially in the domain of graphical abstract reasoning, the advancement of deep learning remains an active area of research. Although deep learning has achieved remarkable success in intelligent vision tasks, elevating machine intelligence to potentially higher levels, the academic community’s research on the abstract reasoning capabilities of deep learning has not ceased. Conversely, this has propelled the emergence of graphical reasoning problems. Graphical reasoning problems pose unique challenges for deep learning, including small and difficult-to-label datasets, the requirement for deep understanding of spatial relationships, shapes, and colors in graphics, demanding strong reasoning and innovation capabilities from models, necessitating a certain level of explanatory ability from models, and posing higher demands on models due to problem complexity and diversity.

To address these challenges, we need to further explore novel model architectures, training methodologies, and optimization strategies. This may encompass directions such as designing more effective deep learning models, refining model training methods, and enhancing dataset quality. Simultaneously, we also need to develop a deeper understanding of the essence and characteristics of graphical reasoning problems so that we can better leverage deep learning techniques to tackle these issues. In summary, while deep learning has made certain strides in graphical abstract reasoning, numerous problems still await our investigation and resolution.

The Ravens Progressive Matrices (RPM) [14] and Bongard problems [12], [13], for example, present learning requirements that span from perceptual processes to inferential capabilities.

### A. RAVEN and PGM

The RAVEN database [15], a distinctive collection of Ravens Progressive Matrices (RPM) problems [14], stands out for its particular design elements. Each RAVEN problem consists of sixteen images, with eight forming the essence of

the problem, termed as the stem, while the remaining eight constitute a pool of alternate choices. Subjects are tasked with selecting appropriate images from this pool, which, together with the stem images, form a 3x3 matrix of graphical patterns. The matrix is characterized by a progressive pattern of geometric images in the row direction, encompassing an underlying abstract concept. Figure 1 presents a concrete instantiation of a RAVEN case’s construction, shedding light on the methodology and general attributes of these problems.

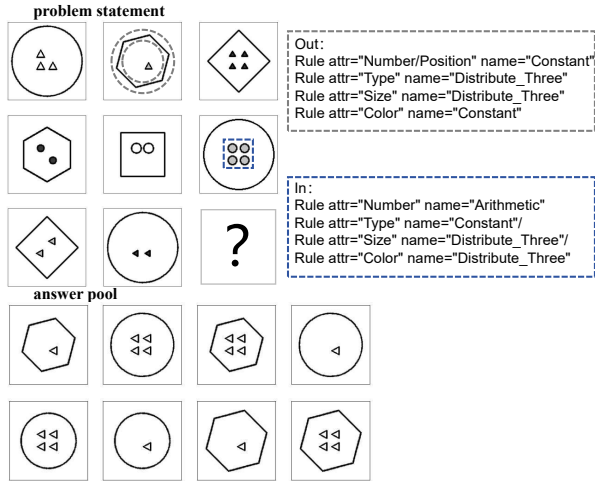


Fig. 1. RAVEN case

Within the design of RAVEN problems, geometric images often encompass human-predefined concepts such as "shape" and "color". However, these concepts are further abstracted in RAVEN problems into a finite, countable, and well-defined set of "visual attributes". The introduction of the term "rule" facilitates the description of how these "visual attributes" progress in a particular manner. It’s worth noting that not all visual attributes are constrained by this "rule"; some may be assigned randomly, posing additional challenges for deep model reasoning.

Constructing a comprehensive RAVEN problem entails initially randomly selecting a rule sample from a predefined rule set. Subsequently, corresponding visual attribute values are devised based on this chosen "rule". For attributes free from rules, their values are assigned randomly. Once these designs are in place, images are rendered according to the derived "attribute" information.

The RAVEN database not only encompasses problems with singular rules but also those with dual rules, elevating the level of difficulty and challenge. Specifically, the RAVEN database includes sub-databases with single rules such as center single, distribute four ( $G2 \times 2$ ), distribute nine ( $G3 \times 3$ ), among others. In problems with a singular rule, the progressive variation of entity attributes within the images is governed by one set of rules. Conversely, in problems involving dual rules, like in center single out center single (O-IC), up center single down center single (U-D), etc., the attribute progression must satisfy two independent rule sets.

The design approach of PGM [16] and RAVEN problems demonstrates a striking resemblance, with both frameworks

employing a problem format consisting of a stem composed of eight images and an answer pool formed by another eight images. It’s noteworthy that within the context of PGM problems, the concept of "rule" assumes a more profound significance. This concept not only delineates the progressive pattern of "visual attributes" along the row direction within the matrix but also imposes constraints on the progressive trend along the column direction. A representative instance of a PGM case is illustrated in the accompanying figure 2.

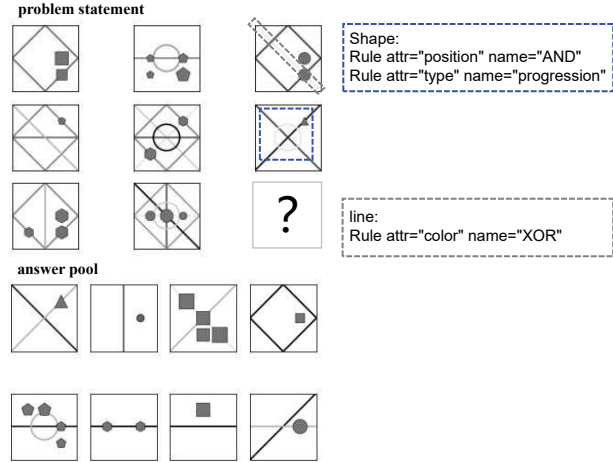


Fig. 2. PGM case

Given this complexity, the challenges associated with RPM problems extend beyond the mere exploration of visual attributes at various levels. They also encompass the crucial task of effectively inducing and learning the progressive patterns exhibited by these "visual attributes". Mastering and comprehending these progressive patterns hold profound implications for successfully tackling RPM problems, thereby underscoring their importance in this cognitive assessment domain.

### B. Bongrad-logo

The Bongard problem [12], [13] stands in stark contrast to the RPM problem, falling under the umbrella of small sample learning problems. Typically, Bongard problems consist of multiple images divided into two distinct groups: primary and secondary. Images within the primary group all convey an abstract concept that is bound by a specific rule, whereas images in the secondary group deviate from these rules in varying degrees. The crux of solving Bongard problems lies in the ability of deep learning algorithms to accurately classify ungrouped images into their respective categories. Notably, Bongard-logo [13] problems, a concrete instantiation of Bongard problems within the realm of abstract reasoning and a combination of a lot of Bongard-logo cases, pose a formidable challenge in terms of inferential complexity. Each Bongard-logo case comprises 14 images, including six images from both the primary and secondary groups, along with two images awaiting classification. The grouping criterion primarily relies on the geometric shapes present within the images and their arrangement. Figure 3 illustrates a representative Bongard-logo case, where every Bongard case consists of two sets of images:

Set A (primary) and Set B (auxiliary). Set A contains six images, with geometric entities in each image adhering to a particular set of rules, while Set B encompasses six images that do not conform to the rules observed in Set A. The task entails assessing whether the images in the test set align with the rules manifested in Set A. The level of difficulty varies depending on the case’s structural complexity.

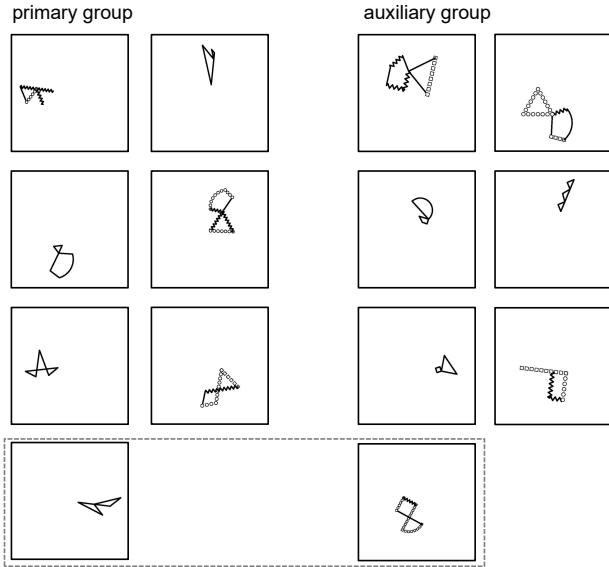


Fig. 3. Bongard-Logo case

Moreover, Bongard-logo problems can be further subclassified into three categories based on the concept domains they encompass: 1) Free-form problems (FF), where shapes are composed of randomly selected action strokes, with each image potentially housing one or two such shapes; 2) Basic shape problems (BA), which require recognition of a combination of one or two shape categories represented within the shape patterns; and 3) High-level concept problems (HD), designed to test a model’s ability to discover and reason about abstract concepts, such as convexity, symmetry, among others. Figure 1 exemplarily presents a specific Bongard-logo case alongside its underlying principles.

## II. RELATED WORK

### A. RPM solver

Discriminative models for image reasoning, such as CoPINet [19], LEN+teacher [18], and DCNet [20], offer diverse solutions with multi-dimensional outputs, focusing on learning differences, latent rules, and comparing disparities. NCD [22], SCL [23], SAVIR-T [24], and neural symbolism systems like PrAE, NVSA and ALANS [25]–[27] incorporate various techniques to improve reasoning accuracy and interpretability. By combining effective methods, RS-CNN and RS-TRAN [28] have achieved impressive results on the RPM problem. Triple-CFN implicitly extracts information on concepts and reasoning units, and “indexes” these reasoning unit information according to the concepts, achieving noteworthy reasoning accuracy. CRAB [29], based on a Bayesian

modeling approach, has established a highly customized “conservatory” that aligns seamlessly with its proprietary methodology, embodied in the creation of a new RAVEN database. This bespoke conservatory, despite forfeiting the inherent core challenges of RAVEN such as solution diversity and uncertainty, has facilitated remarkable breakthroughs for CRAB. Meanwhile, the scientific community eagerly anticipates the profound implications of this innovative approach for future research endeavors.

### B. Bongard solver

Researchers have tackled Bongard problems via three primary methods: language feature models, convolutional neural networks, and generated datasets. Depweg et al. used a formal language and symbolic vocabulary with Bayesian inference, but this struggled with complex problems and had scalability issues [12]. Kharagorgiev and Yun pre-trained on image datasets for feature extraction [30]. Nie et al. experimented with CNNs and meta-learning but had subpar results [13]. These methods have distinct strengths and weaknesses, underscoring the need for more research. Yuan introduced PMoC [31], a probabilistic model that measures the likelihood of auxiliary group samples fitting the main group’s distribution, a novel and effective approach. Notably, Triple-CFN [32] has successfully applied a uniform approach to both Bongard-Logo and RPM problems.

### C. Distribution distance measurement method

The formula for the Wasserstein distance [33] can be expressed as:

$$W(P, Q) = \inf(\sum ||X - Y||) \quad (1)$$

where  $P$  and  $Q$  are two probability distributions, and  $X$  and  $Y$  are random variables sampled from  $P$  and  $Q$ , respectively. Here,  $||X - Y||$  represents the distance between  $X$  and  $Y$ , which can be the Euclidean distance, Manhattan distance, or other suitable metrics. The infimum (inf) denotes the minimum value among all possible mapping strategies. The Wasserstein distance is a measure of dissimilarity between distributions that accounts for the degree of difference between them, particularly suitable for handling non-uniform distributions and considering the shape and structure of the distributions. In the field of machine learning, the Wasserstein distance is widely used in generative models to evaluate the discrepancy between images generated by the generator and real images.

Sinkhorn distance [34] is a metric based on optimal transport, which approximates the Wasserstein distance through the introduction of entropy regularization, leading to increased computational efficiency. This distance satisfies the triangle inequality and is symmetric, but it is not a true distance metric since it converges to the Wasserstein distance only when the regularization term tends to zero. In each iteration, the Sinkhorn algorithm computes a new transportation plan based on the current one and updates the cost matrix, gradually reducing the cost of the transportation plan and approximating the optimal transport solution.

Under certain conditions, the Sinkhorn distance satisfies Lipschitz continuity. Specifically, if we consider two probability distributions with support sets in a compact metric space satisfying certain geometric conditions, the corresponding Sinkhorn distance can be shown to be Lipschitz continuous. This means that there exists a constant  $L$  such that for all probability distributions  $\mu'$  and  $\nu'$ , as well as  $\mu$  and  $\nu$ , the following holds:

$$S(\mu, \nu) \leq L \cdot d(\mu, \nu) + S(\mu', \nu') \quad (2)$$

where  $S$  is the Sinkhorn distance based on the cost function  $c$ , and  $d$  is an appropriate distance between these distributions (such as the Wasserstein distance).

The Lipschitz constant  $L$  typically depends on the choice of regularization parameters and cost functions. In practice, the Lipschitz constant may be difficult to compute directly but can be estimated through numerical experiments. It is worth noting that the Lipschitz constant often relates to the choice of cost function  $c$ . For instance, if  $c$  is a metric in the metric space (such as Euclidean distance), and the geometric properties of the space (like diameter or curvature) meet certain criteria, determining bounds for the Lipschitz constant becomes easier. However, for general cost functions and regularization parameters, determining the Lipschitz constant can be a highly complex task.

When the cost function for Sinkhorn distance is Euclidean distance, its Lipschitz constant depends on parameters of the Sinkhorn algorithm used and characteristics of the dataset, such as size, shape, and distribution. Additionally, Sinkhorn algorithm parameters, like the number of iterations and the weight of the regularization term, influence the continuity properties of the resulting Sinkhorn distance.

Therefore, to determine the Lipschitz constant for Sinkhorn distance with Euclidean distance as the cost function, specific dataset experiments and analyses are necessary to evaluate the continuity properties of the algorithm under different parameter settings. In applications involving Sinkhorn distance, particularly in machine learning and optimization problems, the focus is often on numerical stability and computational efficiency rather than strictly proving Lipschitz continuity or determining the Lipschitz constant. If strict theoretical guarantees are indeed required, detailed analyses of specific problem settings may be necessary.

#### D. Spectral normalization

Spectral normalization [35] is a stabilization technique for deep neural networks, particularly beneficial for generative adversarial networks (GANs). It controls the Lipschitz constant by normalizing weight matrices, ensuring outputs change proportionally to inputs. This regularizes the network, preventing overfitting and instability. In GANs, it stabilizes adversarial training, improving convergence and sample quality. Spectral normalization is computationally efficient and offers a direct way to control network complexity, making it a valuable tool for deep learning practitioners.

#### E. generative model

Wasserstein GAN [36] is a deep learning model that uses the Wasserstein distance as its loss function in Generative Adversarial Networks (GANs) to improve training stability and sample quality. By optimizing this distance, it effectively reduces mode collapse and enhances the realism and diversity of generated data.

DDPM (Denoising Diffusion Probabilistic Model) [9] is a generative model that models the transition from a real image to random Gaussian noise and vice versa to create new images. It involves a forward (diffusion) process adding noise and a reverse (denoising) process restoring the original image. The aim is to generate images ( $x'$ ) that are highly similar to real ones ( $x$ ), emphasizing realism and authenticity.

### III. METHODOLOGY

Both Bongard-logo and RPM problems [14] belong to the category of abstract reasoning problems, which require solvers to possess the ability to extract specific concepts from abstract entities. These specific concepts, compared to lower-level concepts such as “pixel arrangement and configuration styles”, possess a higher level of abstraction and incorporate prior knowledge from human perspectives to varying degrees, encompassing aspects such as shape, size, color, positional relationships, graph concavity and convexity, and graph closure. Bongard-logo and RPM problems employ different questioning approaches aimed at evaluating the solver’s proficiency in extracting and learning these abstract concepts.

This paper presents Lico-Net, a novel baseline model specifically designed for the RPM problem, which achieves remarkable performance in addressing this cognitive challenge. Subsequently, we introduce a fundamental argument that representing abstract and complex concepts as distributions, rather than vectors, is a more suitable approach. Based on this insight, we develop the D3C method. This technique not only enhances Lico-Net’s performance and interpretability on RPM tasks but also elevates the reasoning accuracy of Triple-CFN, a notable deep model that has excelled in Bongard-Logo problems. Recognizing the sources of reasoning difficulties in Bongard-Logo problem, we devise the D2C method. This method is broadly applicable to both RPM and Bongard-Logo challenges, demonstrating improved performance over several baseline models in these domains. Finally, we introduce the D4C method, which targets the essential aspects of abstract reasoning. This approach contributes significantly to advancing our understanding of RPM and Bongard-Logo problems, paving the way for future research in abstract reasoning.

### IV. DISCRIMINATOR OF CASE (DC)

In this section, to enhance our understanding and tackle the RPM (Raven’s Progressive Matrices) problem more effectively, we introduce a new baseline architecture, named Lico-Net. This innovative network is designed to address the unique challenges posed by RPM, leveraging advanced techniques and methodologies to achieve superior performance. Through a rigorous evaluation, we demonstrate the effectiveness of Lico-Net in solving RPM problems, paving the way for future

research in this domain. Furthermore, we delve deeper into the previously established baseline network for the Bongard-Logo problem, critically examining its performance and limitations.

A. A novel baseline, Lico-Net, for RPM problem

The RPM problem requires participants to select answers from an option pool in order to complete a  $3 \times 3$  progressive matrix of images. If the completed matrix adheres to a specific image progressive pattern that can be inferred from the incomplete matrix (problem statement), it is considered a correct answer selection [39]. Therefore, a successful RPM discriminator is expected to be able to identify the rationality of the progression pattern within a complete  $3 \times 3$  progressive matrix.

We require an outstanding baseline, leading us to propose the Lico-Net (link-conception net) as a novel network for RPM solvers. Lico-Net is designed to assess the rationality of the image progression patterns within a complete  $3 \times 3$  RPM matrix, and to represent this rationality through a score. Accordingly, we can sequentially employ all the options provided in an RPM case to complete the problem matrix, leverage Lico-Net to evaluate the progressive rationality of the matrix, and assign scores to the options based on this rationality. This approach allows us to reason and solve RPM problems effectively. The design details of Lico-Net are described as follows.

1) *Perceptron module of Lico-Net* : Aligned with the current consensus among RPM solvers, which emphasizes the need for multi-scale or multi-viewpoint feature extraction from RPM images [23], [24], [28], Lico-Net incorporates the Vision Transformer (ViT) as a perceptron for feature extraction, while preserving the entire output vector, attention results, as multi-view point features. In this paper, we denote the number of viewpoints as  $L$ , a practice similar to that employed in Savirt [24], RS-Tran [28] and Triple-CFN. Lico-Net subsequently processes each viewpoint of extracted feature equally. The perceptron of Lico-Net is illustrated in figure 4.

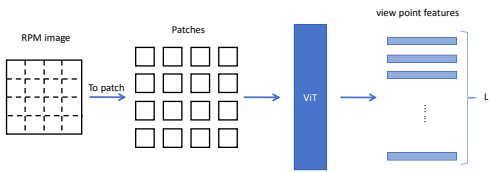


Fig. 4. Perceptron of Lico-Net

2) *Reasoning module of Lico-Net* : The Reasoning module of Lico-Net processes each view point feature generated by the perception module equally and in parallel, resulting in  $L$  sets of inference outcomes. Subsequently, the mean value of these inference results is utilized as the global inference outcome for Lico-Net. The detailed process is described as follows.

For the isometric viewpoint of an completed  $3 \times 3$  progressive matrix, we employ an MLP (Multi-layers perceptron) with a bottleneck structure to extract information from all minimal reasoning units (three images within a row for RAVEN and three images within a row or column for PGM) and obtain

unit vectors. Specifically, we concatenate the representations of all images within a minimal reasoning unit in their inherent order and input them into the MLP. Compared to other structures, the MLP more directly preserves the order of the input representations and its structure is sufficiently simple. The extraction process of unit vector is illustrated in figure 5. Due to the design of RPM problems, typically multiple

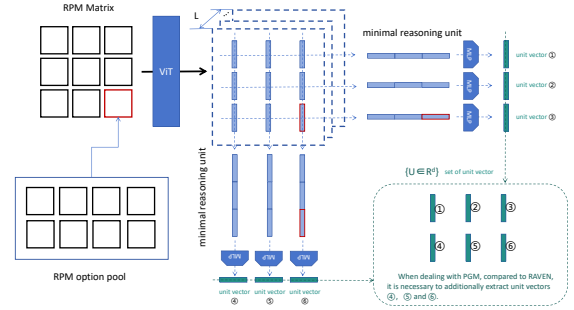


Fig. 5. The extraction process of unit vector

minimal reasoning units must be combined to arrive at the image progression pattern of a RPM matrix. For instance, a RAVEN case requires at least two row unites to discern the case’s pattern, while PGM necessitates at least two row unites and two column unites [39]. It’s worth noting that determining the RPM matrix’s progression pattern doesn’t necessitate all minimal reasoning units; therefore, numerous combination methods of minimal reasoning units exist that are sufficient to identify the pattern. We refer to the combination requiring the least unit vectors as the minimal concept group.

Given that RPM problems might be constrained by multiple independent and decouple patterns, we embed  $N$  optimizable vectors within each minimal concept group (in this paper, we embed two optimizable vectors, with  $N$  being a hyperparameter that can be freely set) and input them into a standard Transformer-Encoder as tokens to compute  $N$  progression pattern vectors for the progressive matrix in the case. Assuming there are  $M$  minimal concept groups, we have thus obtained  $N \times M$  progression pattern vectors under one viewpoint. We denote the progressive pattern vector from a single perspective as  $\{P_{nm} | n \in [1, N], m \in [1, M]\}$ . These vectors have additional purposes to fulfill. This calculation process can be expressed in figure 6. This paper independently

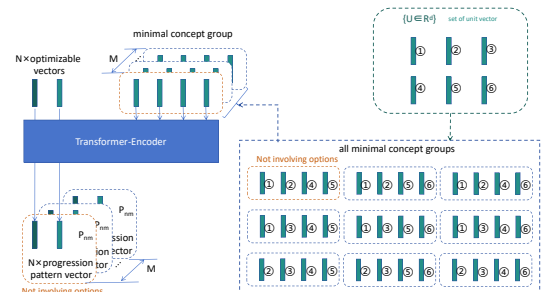


Fig. 6. The extraction process of pattern vector



calculates the scores of each option in the problem under  $N$  distinct pattern vectors.

The  $M$  minimal concept groups can be divided into two categories: those involving options and those not involving options. In this paper, we select the pattern vectors calculated from the concept groups not involving options as queries, and the pattern vectors involving options as keys and values. We then compute the multi-head cross-attention results between them and use a new MLP to score the attention outputs. Since we intentionally introduced  $N$  patterns, we obtain  $N$  scores, which are summed to yield the final score for one viewpoint. This process is illustrated in figure 7. Finally, we

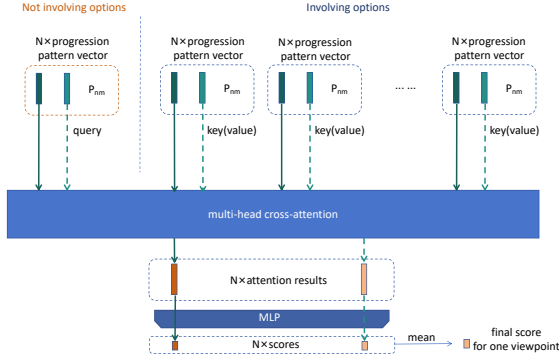


Fig. 7. The calculation process of final score for one viewpoint

calculate the overall score of one option by averaging the scores from all viewpoints. Aligned with the answer logic, we employ the Cross-Entropy loss function to constrain these scores for optimizing Lico-Net. It's worth noting that we treat each dimension of the unit vector as sample results from a distribution and use covariance matrices as additional loss function term to control the correlation between these distributions, aiming to encourage the unit vectors to contain more information. The loss function  $\ell_{cov}$  attached to a batch of the minimal reasoning unit vectors  $\{U_{ij} | i \in [1, b], j \in [1, a]\}$  can be expressed as:

$$\begin{aligned}
 M_{cov}(\{u_{ij} | i \in [1, n], j \in [1, m]\}) \\
 &= \frac{1}{n-1} \sum_{i=1}^n \sum_{j=1}^m (u_{ij} - \bar{u})(u_{ij} - \bar{u})^\top, \\
 \text{where } \bar{u} &= \frac{1}{n} \sum_{i=1}^n \sum_{j=1}^m u_i
 \end{aligned} \tag{3}$$

$$\begin{aligned}
 \ell_{cov}(\{U_{ij} | i \in [1, b], j \in [1, a]\}) \\
 &= \frac{1}{d} \sum M_{cov}(\{U_{ij} | i \in [1, b], j \in [1, a]\})^2 \cdot (1 - I)
 \end{aligned} \tag{4}$$

Where  $b$  represents the batchsize for training the Lico-Net, and  $a$  denotes the count of minimal reasoning units within a single RPM case, which amounts to three in RAVEN and six in PGM.  $I$  represents the identify matrix. And  $d$  represents the dimension of unit vectors  $U_{ij}$ . The entire feedforward process of Lico-Net can be depicted in figure 8.

In summary, after completing the RPM problem matrix with any given option, Lico-Net employs its perception module to

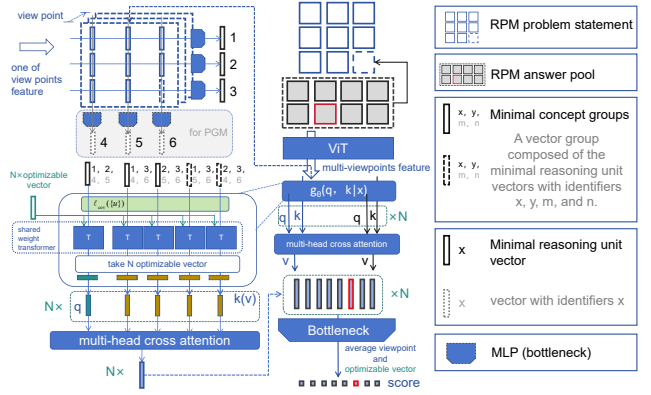


Fig. 8. Feedforward process of Lico-Net

encode each image within the problem matrix from multiple viewpoints, resulting in  $L$  sets of  $3 \times 3$  image representations. The subsequent reasoning module of Lico-Net processes these  $L$  sets of representations in parallel and equally. For any given set of representations, Lico-Net combines them to form all possible  $M$  minimal concept groups. Subsequently, Lico-Net extracts  $N$  progressive patterns from each minimal concept group, totaling  $N \times M$  progressive patterns. Finally, Lico-Net utilizes an cross-attention mechanism to measure the consistency of each progressive pattern expressed by the  $M$  minimal concept groups and reflects this consistency through scores, resulting in  $N$  consistency scores. The final score for the option is determined by averaging these  $L \times N$  consistency scores.

### B. The baseline for Bongard-Logo problem

The cases designers of Bongard-logo drew from high-dimensional human concepts and knowledge, carefully categorizing the Bongard-logo database into three distinct problem types: FF, BA, and HD. It is worth noting that the concept HD is decomposed into NV and CM during testing. This classification allows us to abstractly represent the distribution of the primary group in each Bongard-logo case as  $p_i(x|y)$ , while the distribution of the auxiliary group is denoted as  $q_i(x|y)$ . Here,  $y$  denotes the reasoning type of the case, which can take values from the set FF, BA, HD, and  $i$  represents the case index, ranging from 1 to  $n$ , where  $n$  is the total number of cases. Additionally, we denote the Bongard-Logo images as  $x_{ij}$ . Specifically,  $\{x_{ij} | j \in [1, 6]\}$  represents images in the  $i$ -th primary group, while  $\{x_{ij} | j \in [8, 13]\}$  represents images in the  $i$ -th auxiliary group. Additionally,  $x_{i7}$  represents the test image to be potentially assigned to the  $i$ -th primary group, and  $x_{i14}$  represents the test image to be potentially assigned to the  $i$ -th auxiliary group.

We copy a baseline from Triple-CFN [32], which refers to the baseline as  $f_\theta(z|x)$  that maps samples  $x_{ij}$  to latent variables  $z_{ij}$ . The baseline employs the InfoNCE loss function, which results in the  $f_\theta(z|x)$  being able to solve Bongard-logo to a certain degree. The InfoNCE loss function [41] can be

mathematically expressed as:

$$\begin{aligned} & \ell_{\text{InfoNCE}}(z_{\text{pri}}, \tilde{z}_{\text{pri}}, \{z_{\text{aux}_m}\}_{m=1}^M) \\ &= -\log \frac{e^{(z_{\text{pri}} \cdot \tilde{z}_{\text{pri}})/t}}{e^{(z_{\text{pri}} \cdot \tilde{z}_{\text{pri}})/t} + \sum_{m=1}^M e^{(z_{\text{pri}} \cdot z_{\text{aux}_m})/t}} \end{aligned} \quad (5)$$

Where  $z_{\text{pri}}$  and  $\tilde{z}_{\text{pri}}$  represent distinct samples belonging to the representations in primary group, and  $z_{\text{aux}_m}$  encompasses all  $m$  samples within the auxiliary group.  $m$  denotes the number of negative samples within a minimum learning unit, while  $t$  represents the temperature coefficient, and  $t$  is set  $10^{-3}$ .

This approach fosters a higher degree of similarity between  $z_{\text{pri}}$  and  $\tilde{z}_{\text{pri}}$  compared to the similarity between  $z_{\text{pri}}$  and  $z_{\text{aux}_m}$ , thereby emphasizing the distinction between primary and auxiliary representations. This process aligns with the underlying logic of Bongard-logo. InfoNCE can be construed as a loss function devised for the clustering of vector groups.

This paper reproduces the baseline experiments in Triple-CFN [32], which were originally conducted on the Bongard-Logo using the ResNet18 model. The baseline focuses on learning four concepts in Bongard-Logo — 'FF', 'BA', 'NV', and 'CM' — separately or in combination [32]. To assess the impact of model size on the baseline experimental findings, we have replaced the backbone of the baseline experiments from ResNet18 to ResNet50 and repeated the experiments. The experimental results are presented in Table I, while the feedforward process is illustrated in Figure 9.

The findings indicate that when presented with a combination of databases, both ResNet18 and ResNet50 experience confusion among the four distinct human concepts. The varying degrees of decrease in the models' reasoning accuracy on the FF and BA problems, coupled with the increase in accuracy on the generalization problems NV and CM, both clearly demonstrate this confusion. Furthermore, this confusion cannot be attributed to insufficient network capacity, as even ResNet50, which is more capacious than the ResNet18 used in Triple-CFN's baseline, is subject to the same challenge.

TABLE I  
REASONING ACCURACIES OF DC BASED RESNET BASED RESNET50 ON BONGARD-LOGO.

Model and Data Set	Test Accuracy(%)			
	FF	BA	CM	NV
ResNet18 on Bongard-logo	88.1	97.9	76.0	75.8
ResNet18 on Separated Bongard-logo	97.9	99.0	75.0	72.8
ResNet50 on Bongard-logo	88.9	98.0	76.1	76.0
ResNet50 on Separated Bongard-logo	98.3	99.2	75.3	72.2

After conducting backbone substitution experiments, this paper aligns with the perspective of Triple-CFN [32]. Triple-CFN argues that the identification of image attributes in the Bongard-Logo problem relies heavily on primary and auxiliary samples in specific cases [32], posing challenges due to this context-dependent attribute determination. In other words, the reasoning identity of these images is contingent upon context-specific concepts, leading to multifaceted interpretations of

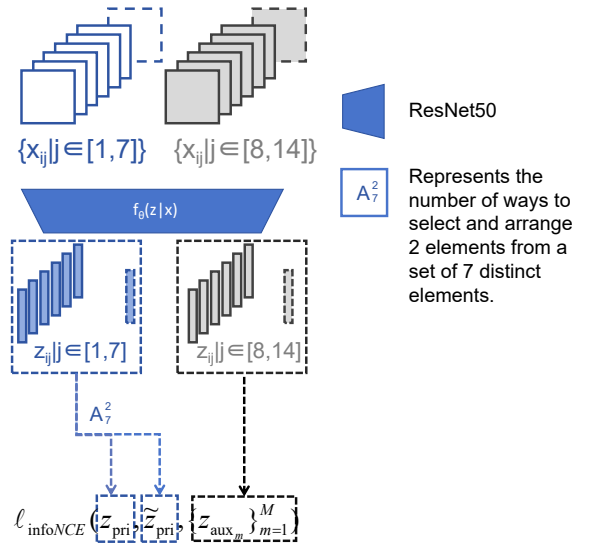


Fig. 9. Feedforward process baseline

image attributes. Consequently, deep networks encounter confusion when processing high-dimensional Bongard-Logo concepts [32]. In contrast, the RPM problem exhibits consistency in its recognition of image attributes, such that a white medium-sized triangle retains its identity regardless of its appearance in any RPM case option pool.

## V. DISTRIBUTION DISTANCE-BASED DISCRIMINATOR OF CASE (D3C)

Using distributions to describe human concepts in abstract reasoning problems for the deep networks is preferable to using vectors. Distributions offer a more comprehensive and nuanced approach to capturing the diversity and uncertainty inherent in human concepts. Human concepts are often ambiguous, polysemous, and subject to varying degrees and fluctuations, which can be challenging to represent using static vectors. In contrast, distributions provide a dynamic and probabilistic framework that can accommodate this inherent variability.

By leveraging distributions to represent human concepts, we can furnish deep networks with richer and more flexible information. This enhanced representational capacity enables the networks to better understand and address the complexity and uncertainty encountered in abstract reasoning problems. For instance, probability distributions can be utilized to depict the range of possibilities and variations associated with a concept, while Gaussian distributions can model the continuity, smoothness and even discreteness of a concept's underlying structure.

### A. D3C for Bongard-Logo

D3C proposes that distributions are more suitable as abstract representations of concepts compared to vectors. Therefore, D3C decides to estimate the concept in each image of a Bongard-Logo case using a deep network in the form of

$f(z|x)$  and represent the concept with a distribution. Finally, the distances between these distributions are measured and used as the distances between concepts. These distances can be naturally applied to solve the Bongard-Logo problem. D3C is a plug-and-play method targeted at solving Bongard-Logo and similar problems for any network in the form of  $f(z|x)$ . Notably, this brings improvements for models such as Triple-CFN and ResNet50.

In practice, this paper hypothesizes that the concepts of the image samples in a Bongard-Logo case follows a Gaussian distribution. We utilize an arbitrary backbone network  $f(z|x)$  to extract the concepts of images within Bongard-Logo cases in form of approximating distribution. To achieve this, we modify the network to output two vectors  $\mu$  and  $\sigma$  instead of a single vector  $z$ , effectively converting  $f(z|x)$  into  $f(\mu, \sigma|x)$ . The encoded vector  $z$  is then divided into two equal-length segments  $\mu$  and  $\log(\sigma^2)$ , which we interpret as the mean and the logarithm of the variance, respectively. This approach normalizes the output vectors into Gaussian distributions and represents concepts as distributions in Bongard-Logo cases. Our method bears resemblance to the Variational Autoencoder (VAE) framework [8]. We argue that using distributions, rather than vectors, to describe image representations offers greater flexibility and accuracy in capturing the underlying complexity and uncertainty of abstract reasoning problems.

With the estimated concepts for each image in the Bongard-Logo cases as distributions, we compute the Sinkhorn distance between these distributions using reparameterization technique [8]. Following the logical structure of each Bongard-Logo case, we impose constraints on these distances for the backbone network  $f(\mu, \sigma|x)$ , aiming to train an effective discriminator. Specifically, we optimize the network by utilizing a binary cross-entropy loss function to enforce constraints on the exponential function of the negative Sinkhorn distance with base  $e$  ( $e^{-D} \in [0, 1]$ , where  $D \in [0, +\infty]$  is the values of Sinkhorn distance), aligning with the case's underlying logic mentioned in DC. This process can be expressed as figure 10. The D3C Method, applied to a batch of Bongard-Logo case distributions encoded by the backbone network  $f(\mu, \sigma|x)$ , can be expressed as follows:

$$\begin{aligned} \ell_{\text{D3C}}(\{z_{ijs} | i \in [1, b], j \in [1, 14], s \in [1, S]\}) \\ = \sum_{i=1}^b \sum_{j=1}^7 \sum_{\tilde{j}=j+1}^7 \text{Sinkhorn}(z_{ijs}, z_{i\tilde{j}s}) \\ + \sum_{i=1}^b \sum_{j=1}^7 \sum_{\tilde{j}=7}^{14} \log(1 - e^{-\text{Sinkhorn}(z_{ijs}, z_{i\tilde{j}s})}) \end{aligned} \quad (6)$$

Where  $b$  is the batchsize of training. The  $\{z_{ijs} | i \in [1, b], j \in [1, 14], s \in [1, S]\}$  represents  $S$  samples drawn from the distribution  $\{\mu_{ij}, \sigma_{ij} | i \in [1, b], j \in [1, 14]\}$  using the reparameterization trick, where the distribution  $\{\mu_{ij}, \sigma_{ij} | i \in [1, b], j \in [1, 14]\}$  is obtained by mapping the Bongard-Logo image  $\{x_{ij} | i \in [1, b], j \in [1, 14]\}$  through the network  $f(\mu, \sigma|x)$ . The network  $f(\mu, \sigma|x)$  is derived from the network  $f(z|x)$  by D3C Method.  $S$  is set to 20, and  $S$  represents the sampling frequency of the reparameterization technique.

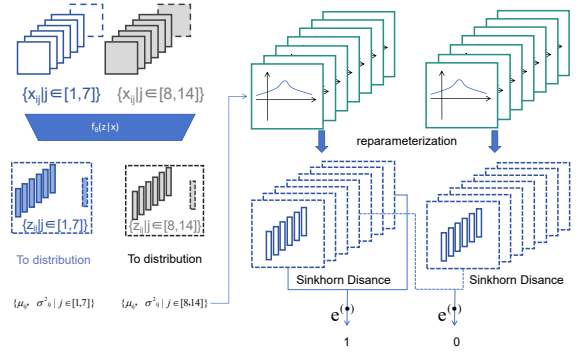


Fig. 10. Feedforward process of D3C

The design of D3C allows for its application to any image encoder that can be abstracted as  $f(z|x)$ . This requirement is met by a wide range of encoders, including those from the ResNet family, ViT, and specialized ones like Triple-CFN, which is particularly suitable for Bongard-Logo problems.

### B. D3C on Lico-Net for RPM

Notably, in contrast to the Bongard-Logo database, both RAVEN and PGM possess well-defined and comprehensive Meta data in the form of (auxiliary) rule labels. These rule descriptions facilitate the construction of a rational concept space, with boundary concepts within the rule labels. This paper introduces the rule labels from the RPM database into the Lico-Net, aiming to enhance the reasoning accuracy and human-perspective rule interpretability of Lico-Net. This process will be implemented by the D3C method.

Within the frameworks of RAVEN and PGM, there is a many-to-one mapping between image progression patterns and their corresponding rules. For instance, both single-step and double-step increments, as well as single-step and double-step decays in image attributes, are all categorized under the ‘progressive’ rule. Therefore, this paper proposes the concept of rules from the RPM database and represent them as distributions while also vectorizing the image progression patterns. This approach is precisely the original idea behind D3C, which posits that describing concepts using distributions is more appropriate than using vectors. We can leverage this approach to naturally constrain the image progression patterns within their corresponding rule distributions, thereby optimizing the deep model’s learning of rules and clarifying the boundaries among various concepts within the data.

In practice for D3C, we utilized a standard Transformer-Encoder to convert the textual descriptions of Meta data into concept vectors  $\{r_k | k \in [1, K]\}$ , where  $K$  represents the count of distinct rule description in Meta data. Specifically, the initial portion of the feature vector is designated as the mean  $\{\mu_k | k \in [1, K]\}$ , whereas the latter half signifies the logarithm of variance  $\{\log(\sigma_k^2) | k \in [1, K]\}$ , effectively distributing the rule descriptions and yielding a set of distributions  $\{\mu_k, \sigma_k^2 | k \in [1, K]\}$ . Lico-Net has inherently achieved the vectorization of image progression patterns, yielding vectors  $\{P_{nm} | n \in [1, N], m \in [1, M]\}$  termed as progression pattern vectors. Consequently, we integrated a constraint term



into Lico-Net, dictating that vectors representing progression patterns should exhibit a high likelihood of adhering to the distribution outlined by their corresponding textual rules, and conversely, demonstrate a low probability of deviation.

A specific RPM case is encoded into  $N \times M$  progression pattern vectors  $\{P_{nm} | n \in [1, N], m \in [1, M]\}$  from  $L$  viewpoints by Lico-Net as aforementioned. To align Lico-Net with the D3C framework, the number of encoding patterns  $N$  in Lico-Net is set according to the instance of the RPM problem, depending on the number of decoupled concepts present in the Meta data of that instance. For example, in PGM, there are two such concepts: shape pattern and line pattern, and  $N$  is set to 2. The special setting of  $N$  in Lico-Net can be viewed as  $N$  slots, which can be aligned with the  $N$  decoupled concepts described in the Meta data, respectively. By synthesizing all perspectives—specifically, by calculating the mean of the progression pattern vectors  $\{P_{nm} | n \in [1, N], m \in [1, M]\}$  across all  $L$  viewpoints—Lico-Net encodes  $N \times M$  vectors, denoted as  $\{\bar{P}_{nm} | n \in [1, N], m \in [1, M]\}$ , representing the full-viewpoint progression patterns. This process can be expressed as:

$$\begin{aligned} & \{\bar{P}_{nm} | n \in [1, N], m \in [1, M]\} \\ &= \frac{1}{L} \sum_{l=1}^L \{P_{nm} | n \in [1, N], m \in [1, M]\}_l \end{aligned} \quad (7)$$

The  $l$  represents the index of viewpoints. The  $\{\bar{P}_{nm} | n \in [1, N], m \in [1, M]\}$  can be treated as  $N$  sets of  $M$  sampling results. This enables the optimization of distribution distances based on the Sinkhorn distance, thereby enhancing the overall performance through D3C framework. Apparently, this paper utilizes the Sinkhorn distance to constrain the distance between  $M$  progression pattern vectors and their corresponding distributions' sampling results. The  $N$  decoupling concept presented in Meta data is employed to concurrently impose constraints on the  $N$  sets of  $M$  progression pattern vectors, and the process of aligning  $\{\bar{P}_{nm}\}$  with the distributional concepts  $\{\mu_k, \sigma^2_k | k \in [1, K]\}$  can be illustrated in figure 11.

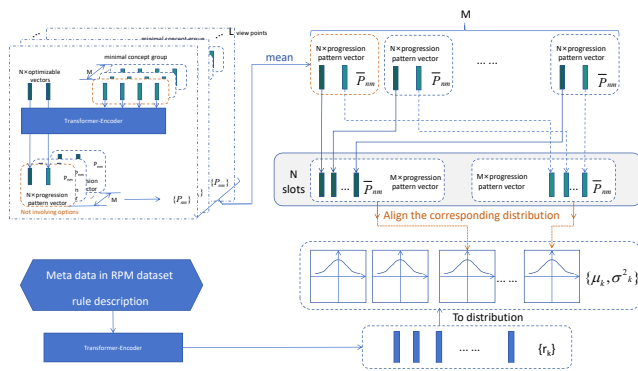


Fig. 11. Feedforward process of D3C

The calculate porcess can be expressed as:

$$\begin{aligned} & \ell_{D3C}(\{\bar{P}_{nm} | n \in [1, N], m \in [1, M]\}, \{r_{ks} | k \in [1, K], s \in [1, S]\}) \\ &= \sum_{n=1, \tilde{k} | n}^N \text{Sinkhorn}(\bar{P}_{nm}, r_{\tilde{k}s}) \\ &+ \sum_{k=1, k \neq \tilde{k} | n=1, \tilde{k} | n}^K \sum_{n=1, \tilde{k} | n}^N \log(1 - e^{-\text{Sinkhorn}(\bar{P}_{nm}, r_{ks})}) \end{aligned} \quad (8)$$

The  $\bar{P}_{nm}$  represents the full-viewpoint progressive pattern vectors encoded by Lico-Net, and  $\{r_{ks}\}$  represents the  $S$  sampling results from the distribution  $\{\mu_k, \sigma^2_k\}$  of the rule description. It is evident that the specific value of  $\tilde{k}$  is contingent upon the description of Meta data corresponding to the particular case of the RPM problem. symbol " $\tilde{k} | n$ " represents that the specific value of  $\tilde{k}$  is depended on  $n$ . This dependency realizes the fact that each slots in Lico-Net are aligned with their corresponding concepts. The Sinkhorn( $\cdot, \cdot$ ) represents the Sinkhorn distance operator. Other logic of symbol in function (8) has mentioned. It becomes evident that we are employing the Binary Cross Entropy (BCE) loss function to impose constraints on the exponential negative Sinkhorn distance result. The feedforward process is illustrated in the figure 12.

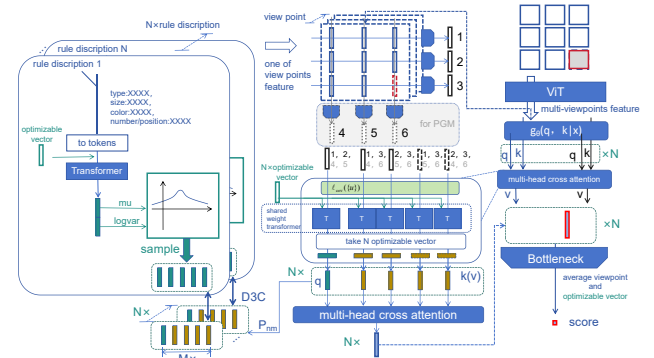


Fig. 12. Feedforward process of Lico-Net aligned with D3C

### C. A low-cost loss function for the D3C, the Hermes for the Zeus

Sampling  $S$  times (where  $S$  is arbitrarily set, and  $S$  is set to 20 for Sinkhorn distance) from the constructed distribution  $\{\mu_k, \sigma^2_k\}$  of concepts in Meta data and yielding  $\{r_{ks} | k \in [1, K], s \in [1, S]\}$ , we calculate the Sinkhorn distance between the progression pattern vectors and these sampling results  $\{r_{ks}\}$ . This Sinkhorn distance approximates the Wasserstein distance, which is currently a linear programming algorithm also known as the Earth Mover's Distance (EMD) algorithm. Typically, this approach requires a substantial number of samples and incurs a considerable computational cost. Even if we treat the  $M$  progression pattern vectors as  $M$  sampling results, it is still difficult to satisfy the prerequisite of extensive sampling in the context of the RPM problem, where  $M$  is set to 9 in PGM and 3 in RAVEN. To reduce computational cost and sampling frequency, this paper employs cosine similarity between vectors as an alternative distance metric norm to the

Sinkhorn distance. Obviously, the cosine similarity satisfies with the *Lipschitz* continuity condition. For the inner product, treating it as a function with one fixed vector, we observe that it exhibits *Lipschitz* continuity. Specifically, given a fixed vector  $v$ , the function  $f(u) = u \cdot v$  is *Lipschitz* continuous with respect to  $u$ , with the *Lipschitz* constant  $L$  being equivalent to the norm of  $v$ . This property is attributed to the inner product's adherence to the Cauchy-Schwarz inequality:  $|u \cdot v| \leq \|u\| \cdot \|v\|$ . Leveraging this inequality, we are able to deduce the underlying inequality:

$$f(u_1) - f(u_2) = |u_1 \cdot v - u_2 \cdot v| = |(u_1 - u_2) \cdot v| \leq \|u_1 - u_2\| \cdot \|v\| \quad (9)$$

In our study, we opted for cosine similarity, considering normalized vectors  $u$  and  $v$ , where  $\|v\|$  and  $\|u\|$  are equal to 1, and Lipschitz constant  $L = \|v\| = 1$ . It is reasonable to choose the mean of cosine similarity between sampling vectors as the distance metric function instead of Sinkhorn distance. The calculate process of new method applied on Bongard-Logo can be expressed as:

$$\begin{aligned} \ell_{\text{D3C-cos}}(\{z_{ijs} | i \in [1, b], j \in [1, 14], s \in [1, S]\}) \\ = - \sum_{i=1}^b \sum_{j=1}^7 \sum_{\tilde{j}=j+1}^7 \sum_{s=1}^S \log \frac{e^{(z_{ijs} \cdot z_{i\tilde{j}s})/t}}{e^{(z_{ijs} \cdot z_{i\tilde{j}s})/t} + \sum_{k=8}^{14} e^{(z_{ijs} \cdot z_{iks})/t}} \end{aligned} \quad (10)$$

The calculate process of new method aligned with Lico-Net can be expressed as:

$$\begin{aligned} \ell_{\text{D3C-cos}}(\{\bar{P}_{nm} | n \in [1, N], m \in [1, M]\}, \{r_{ks} | k \in [1, K], s \in [1, S]\}) \\ = - \sum_{n=1, k|n}^N \sum_{m=1}^M \sum_{s=1}^S \log \frac{e^{(\bar{P}_{nm} \cdot r_{ks})/t}}{e^{(\bar{P}_{nm} \cdot r_{ks})/t} + \sum_{k=1, k \neq \bar{k}}^K e^{(\bar{P}_{nm} \cdot r_{ks})/t}} \end{aligned} \quad (11)$$

The  $t$  is set to  $10^{-6}$  and  $S$  is set to 5 in function (10) and (11). The logic of symbols in function (10) and (11) has mentioned. It is evident that, compared to function (6) and (8), the demand for sampling frequency  $S$  in D3C-cos has been significantly reduced.

From a certain perspective, estimating the distribution distance based on cosine similarity between sampling results can be regarded as a variant of the Wasserstein distance based on cosine similarity that relinquishes the lower bound estimation and possesses a relatively low, fixed Lipschitz constant. Therefore, this method, we called ‘‘D3C-cos’’, cannot precisely quantify the distance between distributions. It serves as a low-cost loss function for constrained inter-distribution distance, serving as a surrogate for the Sinkhorn distance, the Hermes for the Zeus.

The success of such simplification can be attributed, in part, to our modeling of the distribution of pattern descriptions as a Gaussian distribution.

## VI. DYNAMIC DELINEATION OF THE CONCEPT (D2C)

In this section, the paper initially endeavors to introduce novel constraints for the Bongard-Logo discriminators, aiming to enhance their performance. Motivated by these constraints, we incorporate innovative designs into the proposed Lico-Net architecture.

### A. D2C on Bongard-Logo problem

In the Bongard-Logo problem, the determination of image attributes is influenced by the specific contextual concepts associated with each individual case [32]. Distinct concepts require the network to encode specific pixel configurations into differentiated attribute representations, potentially compelling the network to maintain mutually exclusive representation encoding strategies and methods [32]. This scenario often leads to concept confusion within the network, rendering it uncertain about which concept to rely on when processing a Bongard-Logo case [32]. In a nutshell, from the perspective of network, there exists mutual infringement and erroneous coupling among the high-dimensional human concepts in the Bongard-Logo. Therefore, this study aims to develop a methodology that effectively decouples the concepts across different cases within the Bongard-Logo problem. We posit that by successfully decoupling such that distinct cases rely on distinct concepts we may alleviate, to a certain extent, the issue of the network losing concept matching when confronted with a Bongard-Logo problem.

To achieve this objective, we have redefined the concepts within the Bongard-Logo database, representing them as conditional probability distributions  $p_i(x|Y_i)$  and  $q_i(x|Y_i)$ . Here,  $i$  ranges from 1 to  $n$ , denoting each index of the Bongard-Logo cases. Additionally, we introduce the notation  $\{Y'_i | i \in [1, n]\}$  to represent the set of reorganized concepts. It is evident that the number of reorganized concepts corresponds to the number of Bongard-Logo cases. Through this concept reorganization, we strive for mutually exclusive expressions of concepts across all Bongard-Logo cases. In other words, each case is categorized and solved based on its distinct concepts. By establishing a one-to-one correspondence between problem cases and these redefined concepts, we aim to enable the network to avoid uncertainty in determining which concept to rely on when solving a specific case. This approach aims to mitigate the impact of concept confusion on the solution for the Bongard-Logo problem.

To foster concept antagonism between different Bongard-Logo cases, we have revised the data sampling techniques employed in mini-batch training methodologies. Furthermore, an additional loss function term has been devised to facilitate the reassignment of concepts within the network architecture. This approach, termed ‘‘D2C’’ (Dynamic Delineation of Concepts), endeavors to cultivate a state of concept contrast amidst diverse Bongard-Logo cases.

1) *D2C phase 1: The concept delineation method based on a novel dynamic mini-batch sampling technique:* By incorporating an additional ancestral sampling procedure into the traditional mini-batch training sampling methods, this study constructs a Bongard-Logo problem with reorganized concept space for training purposes. This constitutes a hot-swappable approach for training the Bongard-Logo solver, which is designated as phase 1 of the D2C method in this paper.

Specifically, we denote a batch of Bongard-Logo cases as  $\{x_{ij} | i \in [1, b], j \in [1, 14]\}$ , where  $i$  denotes the index of the Bongard-Logo case within a batch, the batch size is  $b$ , and

$j$  represents the sample index within a single Bongard-logo case, with  $j \in [1, 7]$  being the primary samples and  $j \in [8, 14]$  being the auxiliary samples. From this batch of cases  $\{x_{ij}\}$ , we deliberately choose two batches of cases  $\{x_{tj} | j \in [1, 14]\}$  and  $\{x_{\tilde{t}j} | j \in [1, 14]\}$ , ensuring that  $t, \tilde{t}$ , and  $i$  are all distinct. This process can be viewed as ancestral sampling. The extracted primary samples  $\{x_{tj} | j \in [1, 7]\}$  and  $\{x_{\tilde{t}j} | j \in [1, 7]\}$  are then incorporated into  $\{x_{ij}\}$  as auxiliary samples, yielding an expanded set  $\{x_{i\tilde{j}}\}$  where  $\tilde{j} \in [1, 28]$ . Subsequently, The new sample groups  $\{x_{i\tilde{j}}\}$ , which oppose the concepts from different cases compared to their original form, can be fed into any discriminator used to solve Bongard-Logo problems, such as Triple-CFN [32] and PMoC [31]. The feedforward process, as illustrated in the accompanying diagram, involves a strategic misalignment of Bongard-logo problem batches to facilitate ancestral sampling during implementation. The alignment of the D2C phase 1 process with the baseline in DC is illustrated in figure 13.

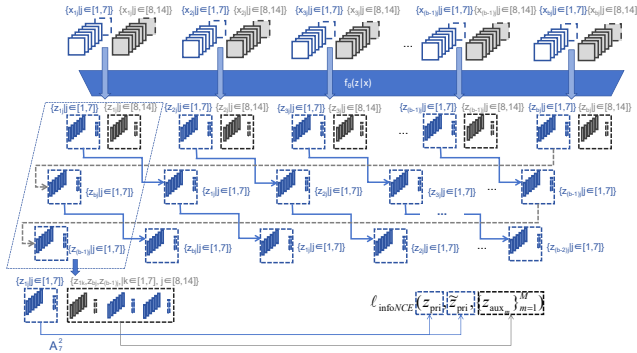


Fig. 13. Feedforward process of D2C phase 1

It is worth emphasizing that the improvement in model performance observed through the aforementioned approach is not solely attributed to an increase in the number of negative examples within each contrastive group. This paper posits that the incorporation of negative examples, which assist in delineating concept boundaries, holds the key to enhancing a model's proficiency in abstract reasoning tasks. Merely augmenting the dataset with insignificant negative examples does not lead to substantial gains in model performance. In an attempt to enrich the dataset, this study generated a substantial amount of Bongard-logo virtual data using DDPM and integrated these as auxiliary data points within the original problems. However, subsequent analysis revealed that this methodology did not tangibly enhance model accuracy.

In summary, the phase 1 of the D2C approach embodies a straightforward yet effective concept: it introduces positive examples from other cases as negative samples in the current case. This strategy sends a clear and additional signal to Bongard-Logo discriminators that distinct problem cases should rely on differing concepts. As a result, the first phase of D2C is widely applicable to various Bongard-Logo discriminators, including Triple-CFN and PMoC.

2) *D2C phase 2: The concept delineation method based on a new loss function term:* This paper posits that, in addition to altering the manner of sampling training data,

establishing an extra loss function to constrain the similarity between the representations of the primary group samples across different cases within a batch of Bongard-Logo training data can implicitly achieve the fundamental objective of this paper.

Specifically, in this paper, we exclusively retain the representation of primary group within the set  $\{z_{ij} | i \in [1, b], j \in [1, 14]\}$ , which specifically correspond to  $\{z_{ij} | i \in [1, b], j \in [1, 7]\}$ . Subsequently, we randomly partition the primary representation of each case within  $\{z_{ij} | i \in [1, b], j \in [1, 7]\}$  into two distinct subsets:  $\{z_{ih} | i \in [1, b]\}$  and  $\{z_{i\tilde{h}} | i \in [1, b]\}$ , where  $\{z_{ih} | i \in [1, b]\} \cup \{z_{i\tilde{h}} | i \in [1, b]\} = \{z_{ij} | i \in [1, b], j \in [1, 7]\}$  and  $\{z_{ih}\} \cap \{z_{i\tilde{h}}\} = \emptyset$ . By taking the mean of the vectors within  $\{z_{ih} | i \in [1, b]\}$  and  $\{z_{i\tilde{h}} | i \in [1, b]\}$ , we derive the corresponding vectors  $\{v_i | i \in [1, b]\}$  and  $\{\tilde{v}_i | i \in [1, b]\}$ . Ultimately, we compute InfoNCE loss function for constraining the similarity among  $\{v_i | i \in [1, b]\}$  and  $\{\tilde{v}_i | i \in [1, b]\}$  as the additional loss function item. The specific calculation process can be explained by:

$$\begin{aligned}
 \mathcal{L}_{D2C}(\{z_{ij} | i \in [1, b], j \in [1, 7]\}) &= - \sum_{i=1}^b \log \frac{e^{(v_i \cdot \tilde{v}_i)/t}}{e^{(v_i \cdot \tilde{v}_i)/t} + \sum_{i=1, \tilde{i} \neq i}^b e^{(v_i \cdot \tilde{v}_{\tilde{i}})/t}} \\
 \text{where } v_i &= \sum \{z_{ih}\}, \tilde{v}_i = \sum \{z_{i\tilde{h}}\} \\
 \text{and } \{z_{ih}\} \cup \{z_{i\tilde{h}}\} &= \{z_{ij} | j \in [1, 7]\}
 \end{aligned} \tag{12}$$

This loss term is to decrease the similarity of primary group representations across different cases. The schematic representation of the feedforward procedure is provided in the figure 14.

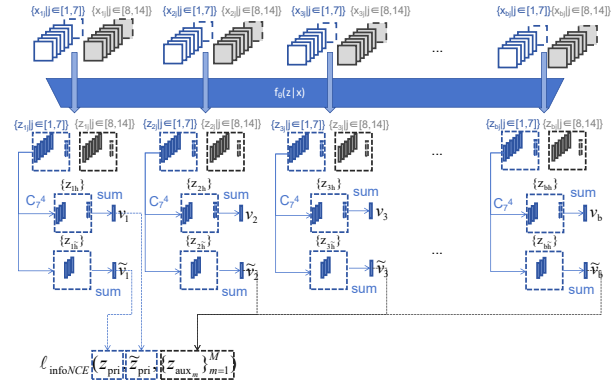


Fig. 14. Feedforward process of D2C phase 2

In essence, the phase 2 of D2C attempts to achieve a similar goal as its first phase by formulating a new loss function, approaching the task from a different angle. Nevertheless, this strategy renders the phase 2 of D2C primarily compatible with backbone that can be abstracted as  $f(z|x)$ . This adaptability enables a majority of image encoders, such as ResNet, ViT, and Triple-CFN [32], to be compatible with the complete D2C methodology. However, the application of PMoC [31], which relies on probability-based measures to assess image identity, is restricted to the first phase of D2C.

### B. D2C on RPM problem

Furthermore, the spirit of D2C method can be integrated with Lico-Net by introducing images from other case statements as negative examples within the cases. However, the application of D2C in RPM discriminators is limited to its phase 1, as it becomes challenging to forcibly apply the phase 2 to these discriminators. This process is illustrated in figure 15.

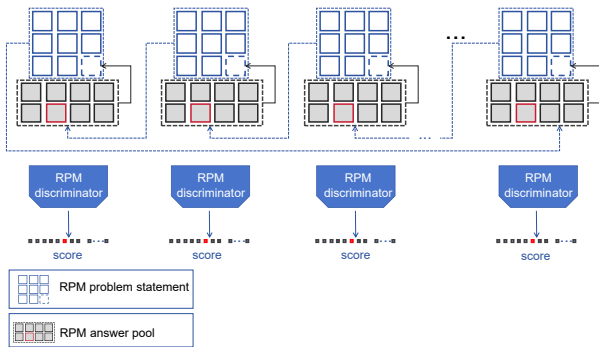


Fig. 15. Feedforward process of Lico-Net aligned with D2C

In summary, D2C is a straightforward approach. In the context of Bongard-Logo, where the determination of image attributes heavily relies on the concepts outlined by the primary and auxiliary groups within each case, D2C addresses this challenge by decoupling the concepts across different cases. Nevertheless, regarding the RPM problem, which emphasizes consistency in image attribute identification, this study maintains a pessimistic outlook on the efficacy of D2C in tackling RPM. In a nutshell, D2C is suitable for addressing the Bongard-Logo problem, where there exists mutual infringement and erroneous coupling of concepts across cases, but it is challenging to apply D2C to the RPM problem, which involves sharing a common set of concepts across cases. It is evident that D2C employs a precautionary approach, aiming to minimize mutual infringement and erroneous coupling among concepts, even at the cost of potential overcorrection. Finally, the D2C and D3C methodologies are not mutually exclusive. Specifically, D2C endeavors to redefine concept boundaries for reasoning problems. According to D3C, representing concepts in the form of distributions is a more plausible approach compared to utilizing vectors.

## VII. DEFENSE-DRIVEN DISCRIMINATION OF DISTRIBUTED CONCEPTS (D4C)

This paper aims to delineate more appropriate concept boundaries for the RPM and Bongard-Logo problems.

### A. Negative samples are not merely intended to confound the discriminator

This paper posits that it is worthwhile to consider the significance of positive and negative examples in abstract reasoning problems. Suppose that the correct solutions to each case in a reasoning problem follow a Gaussian distribution. Given that some reasoning problems may have multiple correct

solutions, it is also possible that the distribution is a mixed Gaussian distribution. This is exemplified in datasets such as OIG and D9 from Raven database. One of the core challenges in RPM problems lies in the existence of multiple correct answers. While CRAB has eliminated this core difficulty through data cleaning in the RAVEN dataset, it has achieved noteworthy results on the cleaned version.

Currently, existing discriminative models for solving RPM and Bongard-Logo problems often adhere to a pattern where positive examples yield high probabilities when substituted into the case’s problem statement, while negative examples yield low probabilities. In a nutshell, they are models with probabilistic labeling scheme. We can view this pattern in the following way: the discriminator constructs a solution distribution for the cases presented in abstract reasoning problems. Within this distribution, positive examples are assigned higher probabilities, whereas negative examples are assigned lower ones. The endeavor to train the discriminator can be conceptualized as a process of optimizing and fine-tuning the solution distribution, with the ultimate objective of aligning it more closely with the underlying distribution of correct solutions for the given cases. Using positive and negative examples to estimate a Gaussian distribution through the cross-entropy loss function can be seen as leveraging them to optimize the following function:

$$-\log(p(x, \mu, \sigma)) = \frac{(x_i - \mu_i)^2}{2\sigma_i^2} - \log(|\sigma_i|) - \frac{1}{2} \log(2\pi) \quad (13)$$

Where  $x$  represents the positive or negative samples,  $\mu$  and  $\sigma$  represent the mean and standard deviation of the Gaussian distribution separately. It can be observed that when positive samples are substituted into the formula, we aim for the smallest possible result, which corresponds to minimizing the mean squared loss between sample  $x$  and the mean of the correct solution  $\mu$ . Conversely, when negative samples are substituted, we desire the largest possible result, equivalent to minimizing the standard deviation  $\sigma$  of the respective segment.

Therefore, this paper posits that in reasoning problems, the establishment of positive examples aids deep models in estimating the mean of the correct solution distribution, while negative examples serve to estimate the variance. The variance represents the distance between the boundaries of the distribution and its center. Correspondingly, we posit that negative examples play a crucial role in abstract reasoning tasks, serving to delimit the concepts presented in each case. This underscores the significance of establishing both positive and negative examples in abstract reasoning problems. This significance reflects a despairing fact that the upper limit of the discriminator’s reasoning accuracy in this abstract reasoning problem is determined by the quality of positive and negative examples in the question.

### B. High-quality negative samples lead to more rigorous concept boundaries

The D2C methodology proposed in this study has established a novel problem boundary for deep networks by means

of resampling negative samples and incorporating a fresh loss function. Experimental findings tentatively indicate that this boundary is better suited for scenarios characterized by the absence of concept supervision signals, as compared to the boundaries delineated by the original negative samples in Bongard-Logo. Nonetheless, the precise tightness of the new boundary remains indeterminate.

In essence, D2C introduces a new variance to the solution distribution of the network, the magnitude of which relative to the variance of the correct solution distribution is indeterminate. In the context of the Bongard-Logo challenge, the variance provided by D2C appears closer to that of the correct solution distribution in the absence of concept supervision signals, as compared to the variance described by the original negative samples.

Evidently, the efficacy of D2C is contingent upon specific dataset attributes. As anticipated, empirical evidence suggests that this approach may be insufficient for delineating precise boundaries within the framework of the RPM problem. Contrary to the Bongard-Logo paradigm, RPM problems postulate a shared set of core concepts across distinct cases, ensuring discreteness and stability. This shared nature precludes the utility of methods like D2C in addressing RPM challenges. Specifically, image properties within RPM cases are rigidly governed by definitions of “rules” or “progressive patterns,” maintaining consistent attributions across all cases.

The Bongard-Logo problem exhibits varying identifications and determinations of image attribute due to differing clustering bases among cases, thereby augmenting problem complexity and difficulty. Incorporating positive samples from other cases as negative examples can, to some extent, delineate concept boundaries between distinct cases, adhering to a cautious approach aimed at minimizing concept infringement. However, this strategy proves inapplicable in addressing challenges presented by RAVEN and PGM due to substantial disparities across multiple dimensions.

In summary, the success of D2C in addressing the Bongard-Logo problem can be attributed to its indirect enhancement of the quality of negative samples within Bongard-Logo cases. Conversely, its limitations in tackling the RPM problem can also be ascribed to its insignificant improvement in the quality of negative examples within RPM scenarios. To address the limitations inherent in the D2C approach, this paper introduces the D4C (Defense-Driven Discrimination of Distributed Concepts) method. The underlying idea of D4C is to generate higher-quality negative samples and samples within abstract reasoning problems. This approach aims to delineate a more appropriate problem boundary for the discriminator as compared to the original problem setup in abstract reasoning. By leveraging novel mechanisms and strategies, D4C aims to deliver more precise and reliable definitions of concept boundaries and foster further advancements in the realm of abstract reasoning.

### C. Impelmention of D4C method

The D4C methodology proposed in this paper emphasizes on devising a more suitable concept boundary for both RPM

and Bongard-Logo discriminators, aiming to enhance their problem-solving capabilities. To achieve this objective, a distinctive approach centered on the generation of confusing samples is introduced. These samples are intentionally designed to challenge and improve the discriminator’s accuracy. A dedicated generator has been devised to carry out this generation process. Through iterative defense against attacks launched by this generator, the discriminator progressively refines its discrimination and classification skills, leading to overall performance enhancement in both areas. Specifically, within this study, a generator has been tailored to augment the capabilities of two distinct Bongard-Logo discriminators: PMoC and Triple-CFN. Additionally, this generator can also be directly utilized for the refinement of Lico-Net. Nevertheless, acknowledging the inherent disparities between RPM problems and Bongard-Logo challenges, additional designs have been incorporated into the generator to cater more effectively to the refinement requirements of Lico-Net.

In this section, we delve into the design of the discriminator and generator within the D4C framework as it pertains to the Bongard-Logo and RPM problems.

1) *discriminator for Bongard-logo*: Effective Bongard-Logo discriminators abound, with our preceding works, such as PMoC and Triple-CFN, achieving notable successes. These discriminators seamlessly integrate with the D2C and D3C methodologies proposed in this study, and pertinent experiments have been conducted to explore their combinations. These discriminators excel in accurately identifying and classifying Bongard-Logo cases, significantly contributing to the advancement of research in this domain.

Regarding discriminators capable of handling adversarial tasks, the Wasserstein GAN, a prominent adversarial generative network, poses a noteworthy requirement. The discriminator must undertake the task of measuring the distance between samples generated by the generator and real samples. This necessitates that the discriminator satisfies Lipschitz continuity to a certain extent.

In this study, the choice of PMoC, constrained by spectral normalization, as the discriminator for the D4C method on Bongard-logo is motivated by its explicit measurement of the distance between auxiliary and primary group sample distributions. Conversely, the task of Triple-CFN is relatively more intricate as it considers not only the distance between primary and auxiliary samples but also the distance among primary samples. Consequently, compared to PMoC, this study entails more elaborate designs for the generator of Triple-CFN.

2) *generator for Bongard-logo*: In this paper, we argue that instead of forcing the generator to produce samples that can confuse the discriminator, it is more effective to generate representations of confusing samples, referred to as confusing representations. This approach reduces the computational burden on the network, as measured by intuitive metrics such as computational complexity.

For the Bongard-Logo problem, we model the overall distribution as a mixture of Gaussian distributions. Within this framework, each individual primary group in a Bongard-Logo case is represented as a separate Gaussian distribution. Consequently, the D4C generator designed for the Bongard-



Logo problem exhibits a relatively straightforward structure. The generator aims to encode a distribution based on the representations of the primary groups in a given Bongard-Logo case, ensuring that any representation sampled from this distribution is capable of effectively confusing the discriminator.

Specifically, we employ a standard Transformer encoder to encode a Gaussian distribution based on the representations of the primary samples in a Bongard-Logo case, along with an optimizable vector. This encoding approach bears similarity to D3C, wherein we extract the optimizable vector from the attention results and process it through a linear feed-forward layer to obtain the mean and logarithm of variance for the Gaussian distribution. Subsequently, we sample multiple representations from this distribution as confusing representations to challenge the discriminator, which must exert maximum effort to counter them. The generator’s training objective is to generate representations for Bongard-Logo cases that achieve higher scores in the discriminator compared to the representations of the original negative examples in the case. Conversely, the discriminator’s training objective is unambiguous: to classify these generated representations as negative examples. The aforementioned approach can be seamlessly applied to the PMoC model, providing a direct and effective means of enhancing its performance. The alignment between the generator and PMoC is illustrated in Figure 16. In this

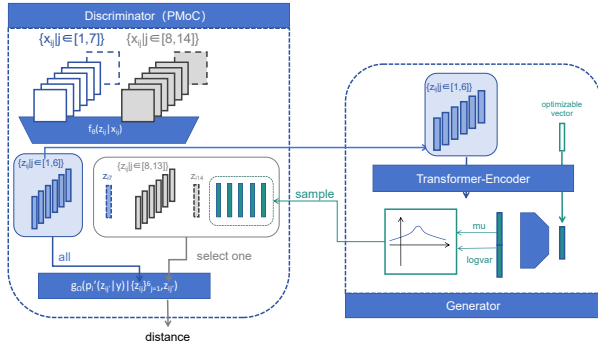


Fig. 16. Feedforward process of D4C aligned with PMoC on Bongard-Logo

figure, the “ $f_{\theta}(z_{ij}|x_{ij})$ ” and “ $g_w(p'_i(z_{ij}|y)|\{z_{ij}\}_{j=1}^6, z_{ij}')$ ” represent the perceptron and logic calculation modules in PMoC, respectively [31].

For the generator in Triple-CFN, it is essential to decay the generated representations. Specifically, when the generator with the aforementioned structure produces a confusing representation for Triple-CFN, this confusing representation must be weighted and summed with the representations in the auxiliary group. After taking the average of the representations in the auxiliary group, it is weighted and summed with the confusing representation in a ratio of 0.9 : 0.1 to decay the confusing representation. This decay process is necessary due to the mechanism of Triple-CFN, which defines the identity of an image based on the direction of its representation. This mechanism makes it easier for a generator based on the Transformer encoder to generate realistic confusing representations, potentially causing Triple-CFN to collapse. Therefore, we have designed the aforementioned decay process. The alignment

between the generator and Triple-CFN is illustrated in Figure 17. In this figure, “ $f_{\theta}(z_{ij}|x_{ij})$ ” represents the encoder in Triple-CFN.

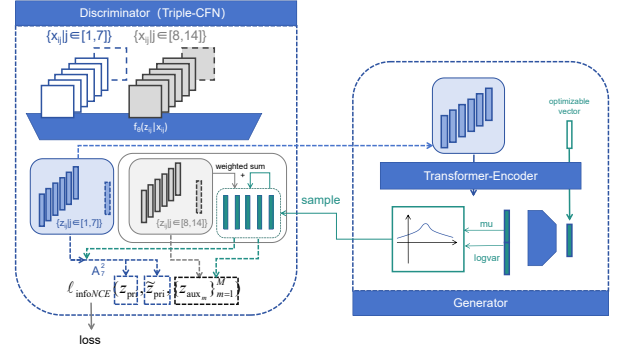


Fig. 17. Feedforward process of D4C aligned with Triple-CFN on Bongard-Logo

3) *discriminator of RPM*: In addressing Raven’s Progressive Matrices (RPM) problems, this study places significant confidence in the Lico-Net model, considering it as an exceptional benchmark. It is anticipated that the application of spectral normalization will enhance the performance of Lico-Net, positioning it as a highly suitable discriminator for the D4C methodology.

However, Lico-Net will encounter challenges posed by the generator, which produces confusing representations aimed at completing the  $3 \times 3$  reasoning matrix. To address these challenges, Lico-Net will undertake an assessment of the internal consistency within the progressive patterns of the  $3 \times 3$  reasoning matrix, which are completed by these confusing representations. Any inconsistencies or irregularities identified within these representations will be flagged as negative samples, indicating incorrect responses. Through this rigorous process, Lico-Net strives to accurately identify and reject perplexing representations, thereby augmenting its overall precision and reliability.

4) *generator of RPM*: Unlike the Bongard-Logo problem, the answer to a single case in the RPM problem exhibits non-uniqueness, and thus can be represented as a mixture of Gaussian distributions. Therefore, our aspiration is to tailor a generator for the D4C method within the RPM context, capable of encoding a distribution that reflects this mixed Gaussian nature. In this paper, we employ a glove-shaped network to simulate the process of sampling from such mixed Gaussian distributions.

Specifically, we utilize a standard Transformer-Encoder to process the representations of all problem images in an RPM case, alongside  $W$  optimizable vectors (where  $W$  is a hyperparameter) and a stochastic promoter. Notably, when these  $W+1$  vectors are arranged together, they resemble the shape of a glove. The promoter is a vector sampled from a multivariate Gaussian distribution, wherein the mean is optimizable while the variance is fixed at 1.

It is worth noting that we have devised a novel positional encoding embedding approach for the Transformer-Encoder, which serves as the backbone of our RPM generator. This

encoding aims to restore the  $3 \times 3$  image arrangement characteristic of the RPM problem matrix. For the PGM (Progressive Graph Matching) problem, our positional encoding scheme assigns unique encodings to images located on the diagonal and upper triangular regions within the problem matrix of a given PGM case. Correspondingly, the positional encodings for images in the lower triangular region are symmetrical with respect to the diagonal, mirroring the encodings of their counterparts in the upper triangular region. However, it should be acknowledged that this paper does not demonstrate the superiority of D4C on the relatively less challenging RAVEN dataset.

Moving on to the main topic, after obtaining attention results from the Transformer-Encoder, we extract  $W$  optimizable vectors from these results and process them into  $W$  distributions using a linear layer, as mentioned earlier. Following the extraction of the promoter, it is processed into a probability output using a linear layer and hard-gumbel-softmax activation, yielding highlighted probabilities for the  $W$  distributions. Subsequently, we sample representations, referred to as confusing representations, from the highlighted distributions each time. In the technical implementation, we employ the reparameterization trick to draw samples from each distribution, resulting in  $W$  sampling outcomes. We then perform a weighted sum of these sampling results using the hard-highlighted probabilities processed by the hard-gumbel-softmax, thus completing the entire mixed-Gaussian sampling process. The methodology outlined in this paper for modeling and training the network is coined as "D4C glove-train". A more detailed illustration of the forward process is provided in the accompanying figure referenced as 18.

The training objective of the glove-shaped generator remains consistent: to produce confusing representations that achieve higher scores in the discriminator compared to the original negative examples provided by the dataset. Conversely, the discriminator aims to resist the interference posed by these confusing representations.

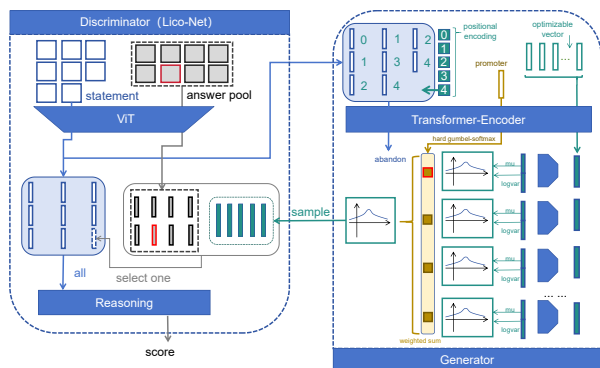


Fig. 18. Feedforward process of D4C on RPM problem

Finally, in the realm of abstract reasoning problems, particularly those involving generating answer samples, this paper believes that the D4C approach can also make valuable contributions. This opens up new avenues of exploration for future work, presenting challenges that are yet to be tackled.

## VIII. EXPERIMENT

All experiments conducted in this paper were programmed in Python, utilizing the PyTorch [43] framework.

### A. Experiment on RAVEN

Initially, we conducted experiments with Lico-Net on both RAVEN [15] and I-RAVEN [37] datasets to demonstrate its inherent potential. To ensure a fair comparison between excellent models, all experimental settings and equipment in this study were kept consistent with those of RS-Tran [28] and Triple-CFN [32], including data volume, optimizer parameters, data augmentation methods (such as reducing the RAVEN image size to  $80 \times 80$ ), batch size, and other relevant hyperparameters.

TABLE II  
REASONING ACCURACIES ON RAVEN AND I-RAVEN.

Model	Test Accuracy(%)							
	Average	Center	$2 \times 2$ Grid	$3 \times 3$ Grid	L-R	U-D	O-IC	O-IG
SAVIR-T [24]	94.0/98.1	97.8/99.5	94.7/98.1	83.8/93.8	97.8/99.6	98.2/99.1	97.6/99.5	88.0/97.2
SCL [23], [24]	91.6/95.0	98.1/99.0	91.0/96.2	82.5/89.5	96.8/97.9	96.5/97.1	96.0/97.6	80.1/87.7
MRNet [21]	96.6/-	-/-	-/-	-/-	-/-	-/-	-/-	-/-
RS-TRAN [28]	98.4/98.7	99.8/100.0	99.7/99.3	95.4/96.7	99.2/100.0	99.4/99.7	99.9/99.9	95.4/95.4
Triple-CFN [32]	98.9/99.1	100.0/100.0	99.7/99.8	96.2/97.5	99.8/99.9	99.8/99.9	99.9/99.9	97.0/97.3
Triple-CFN+Re-space [32]	99.4/99.6	100.0/100.0	99.7/99.8	98.0/99.1	99.9/100.0	99.9/100.0	99.9/99.9	98.5/99.0
Lico-Net	99.5/99.7	100.0/100.0	99.7/99.8	98.2/99.2	99.9/100.0	99.9/100.0	99.9/99.9	98.8/99.2

An interesting observation from the Table II indicates a consensus among existing excellent RPM solvers, including Lico-Net. Specifically, these solvers exhibit differing values of reasoning accuracy when tackling the RAVEN [15] and I-RAVEN [37] datasets. The I-RAVEN dataset was designed to address certain limitations in the option pool configuration of RAVEN by introducing improvements to its negative example setup. These enhancements include, but are not limited to, increasing the number of attributes that are altered in the negative examples and augmenting the magnitude of attribute deviations within them. However, from a human perspective, such additional setups do not alter the difficulty level of reasoning, and thus do not make I-RAVEN any harder or easier compared to RAVEN. This paper speculates that the disparate outcomes achieved by these models on RAVEN and I-RAVEN could potentially be attributed to the superior quality of negative examples present in the I-RAVEN dataset compared to those in RAVEN. Such phenomena echo the D4C's spirit.

### B. Experiment on Bongard-Logo

We conducted experiments on Bongard-Logo using ResNet50 and Triple-CFN [32] as backbones for D2C, D3C(-cos), and D4C and using PMoC [31] as backbone for D2C and D4C. PMoC, a probabilistic labeling model, does not meet the requirements of D3C(-cos), as D3C(-cos) demands a backbone in the form of  $f(z|x)$ . The experimental results are presented in the table III.

Upon observing the results presented in the table III, we found that D2C, D3C, and D3C-cos made considerable contributions in the Bongard-Logo task. As can be seen in the table III, replacing D3C with D3C-cos to integrate with

ResNet50 would not significantly affect performance. We argue that, from a results-oriented perspective, D3C-cos can be considered as an effective alternative to D3C. Notably, we did not conduct an experiment with Triple-CFN+D3C and Triple-CFN+D2C+D3C. This is because the large number of Triple-CFN parameters makes integrating the D3C approach impractical on our current experimental equipment. This was the driving force that led us to propose D3C-cos as an alternative to D3C in this paper.

TABLE III  
REASONING ACCURACIES OF MODELS ON BONGARD-LOGO.

Model	Accuracy(%)				
	Train	FF	BA	CM	NV
SNAIL	59.2	56.3	60.2	60.1	61.3
ProtoNet	73.3	64.6	72.4	62.4	65.4
MetaOptNet	75.9	60.3	71.6	65.9	67.5
ANIL	69.7	56.6	59.0	59.6	61.0
Meta-Baseline-SC	75.4	66.3	73.3	63.5	63.9
Meta-Baseline-MoCo [42]	81.2	65.9	72.2	63.9	64.7
WReN-Bongard	78.7	50.1	50.9	53.8	54.3
SBSD	83.7	75.2	91.5	71.0	74.1
PMoC	92.0	90.6	97.7	77.3	76.0
Triple-CFN	93.2	92.0	98.2	78.0	78.1
ResNet50 (infoNCE baseline)	92.0	88.9	98.0	76.1	76.0
ResNet50+D2C	92.6	90.5	98.2	77.0	77.2
ResNet50+D3C	92.3	90.6	98.3	76.5	76.8
ResNet50+D2C+D3C	93.0	<b>91.0</b>	98.5	77.5	<b>77.5</b>
ResNet50+D3C-cos	92.1	90.2	98.2	76.9	76.4
ResNet50+D2C+D3C-cos	92.9	90.8	98.4	<b>77.5</b>	77.4
ResNet50+D4C	<b>93.2</b>	90.8	<b>98.5</b>	77.2	77.3
Triple-CFN+D2C	93.9	92.7	98.5	78.2	78.5
Triple-CFN+D3C-cos	93.7	92.5	98.3	78.2	78.2
Triple-CFN+D2C+D3C-cos	94.1	<b>93.0</b>	98.5	78.2	78.6
Triple-CFN+D4C	<b>94.3</b>	92.8	<b>98.8</b>	<b>78.7</b>	<b>79.0</b>
PMoC+D2C	92.5	91.2	98.0	77.7	76.7
PMoC+D4C	<b>93.0</b>	<b>92.6</b>	<b>98.2</b>	<b>78.0</b>	<b>77.5</b>

Additionally, D4C has imparted varying degrees of improvement to Triple-CFN, ResNet50, and PMoC, with its effectiveness rivaling that of the combined application of D2C and D3C. However, D4C did not yield an ideal improvement on the FF concept for the Bongard-logo problem when applied to Triple-CFN and ResNet50. This study hypothesizes that the suboptimal performance may be attributed to the fact that D4C was specifically designed and tailored for discriminative models with a probabilistic labeling scheme. Conversely, Triple-CFN and ResNet50 do not inherently adhere to such a framework. It has been mentioned that when integrating D4C with Triple-CFN and ResNet50, a decay mechanism was incorporated. This mechanism is a compromise made by D4C to accommodate the non-probabilistic labeling scheme of these models. From the perspective of experimental results,

this decay mechanism does not appear to be a fully developed mechanism. Exploring more advanced designs to facilitate the adaptation of D4C to non-probabilistic labeling models, such as Triple-CFN, deserves attention as future work. In contrast to Triple-CFN, PMoC [31] serves as an intuitive probabilistic labeling model for the Bongard-Logo problem. Correspondingly, D4C provides a more significant enhancement when applied to PMoC, owing to its scheme.

D4C demonstrated improvement and contribution, validating the effectiveness of defining tighter problem boundaries for the model with a probabilistic labeling scheme. To integrate D4C with Triple-CFN, we devised a representation decay mechanism that, despite its imperfections, is sufficiently effective. This approach warrants further investigation and development in future research.

Finally, this paper notes that augmentation experiments were conducted for both PMoC [31] and Triple-CFN [32]. These experiments involved expanding the data volume of the Bongard-Logo dataset using data augmentation techniques, specifically including rotation and flipping. It should be emphasized that these data augmentation techniques do not explicitly alter the diversity of concepts or the proportion between concepts inherent in the Bongard-Logo dataset [31]. Rather, the aim of these experiments was to investigate the potential of the models with a larger dataset. Since PMoC posits that Transformer-based visual processing models require substantial data as a foundation, a point also echoed by ViT [17] and RS-Tran [28]. Furthermore, both PMoC and Triple-CFN agree that the utilization of these data augmentation methods serves to enrich the expressions of concepts at the pixel level, thereby challenging the network’s abilities to summarize, derive, accommodate, and invert concepts [31], [32]. This paper conducted experiments to verify the effectiveness of D4C with the expanded dataset. The results are recorded in Table IV.

TABLE IV  
REASONING ACCURACIES OF D4C ON AUGMENTED BONGARD-LOGO.

Model	Accuracy(%)				
	Train	FF	BA	CM	NV
PMoC	94.5	92.6	98.0	78.3	76.5
Triple-CFN	94.9	93.0	99.2	80.8	79.1
PMoC+D4C	96.0	95.2	99.2	84.8	82.8
Triple-CFN+D4C	97.7	94.8	99.6	82.8	83.1

The results presented in Table IV demonstrate that the integration of D4C into PMoC, which is under a probabilistic labeling scheme, has led to a significant enhancement in performance. The increase in data volume has enabled D4C to further narrow the gap between PMoC and Triple-CFN.

### C. Experiment on PGM

In this paper, we conducted experiments related to LicoNet on PGM. And the results are recorded in Table V. From the experimental results presented in Table V, several

TABLE V  
REASONING ACCURACIES OF MODELS ON PGM.

Model	Test Accuracy(%)
SAVIR-T [24]	91.2
SCL [23], [24]	88.9
MRNet [21]	94.5
RS-CNN [28]	82.8
RS-TRAN [28]	97.5
Triple-CFN [32]	97.8
Triple-CFN+Re-space layer [32]	98.2
Triple-CFN+Re-space layer+D2C	98.3(98.25)
Lico-Net	98.5(98.52)
Lico-Net+D2C	98.5(98.53)
D4C (with Lico-Net as the backbone)	98.7(98.70)
D4C glove-train(with Lico-Net as the backbone)	<b>98.8(98.82)</b>
RS-Tran+Tranclip [28]	99.0
Meta Triple-CFN [32]	98.4
Meta Triple-CFN+Re-space layer [32]	99.3
Lico-Net+D3C <sup>-</sup>	99.3(99.30)
Lico-Net+D3C	<b>99.4(99.35)</b>
Lico-Net+D3C-cos	<b>99.4(99.38)</b>

notable phenomena emerge. In Triple-CFN, both progressive patterns and minimal reasoning units are positioned at the same logical level [32]. However, a significant design flaw arises from the mismatch in the logical hierarchy between these patterns and units. More specifically, progressive patterns often require the combined expression of multiple minimal reasoning units. Despite this limitation, Triple-CFN still stands as an impressive model. Naturally, leveraging the inductive bias inherent to the RPM problem as the guideline in its design, Lico-Net has achieved even more remarkable results than Triple-CFN in the RPM challenges.

The combination of Lico-Net and D2C, and the combination of Triple-CFN and D2C, did not bring significant improvement, with the enhancement only reflected in the percentile of reasoning accuracy. This phenomenon was anticipated in this paper, as we believe it is due to the difference between RPM and Bongard-Logo problems. In RPM problems, different cases share the same concept space and attribute recognition method. The D2C approach, designed to address issues of concept interference and erroneous coupling among cases, is not applicable to RPM problems.

However, the combination of D4C and D4C glove-train significantly improved Lico-Net’s performance. Additionally, the glove-shaped generator proved to be more suitable for generating negative representations of RPM problems for Lico-Net and enabling it to achieve further refinement. The core innovation of this paper, D4C, has yielded promising results on both the RPM and Bongard-Logo problems, demonstrating the significant contribution of this work.

The combination of Lico-Net and D3C is noteworthy. To validate the theme of D3C, we applied both D3C and D3C-

cos to Lico-Net. Through experimentation, we found that D3C and D3C-cos brought improvements to Lico-Net. To demonstrate the effectiveness of D3C’s approach to describing abstract concepts through distributions, this paper conducted ablation experiments using “Lico-Net+D3C<sup>-</sup>”. Unlike “Lico-Net+D3C”, which encodes the description of image progressive patterns into distributions using a Transformer-Encoder, “Lico-Net+D3C<sup>-</sup>” encodes them into vectors. To simplify, instead of dividing the encoded representation into  $\mu$  and  $\log\text{var}$ , we directly utilize the representation as a vector. Furthermore, the cosine distance between progressive pattern vectors  $\{\bar{P}_{nm}\}$  and the vectorized pattern description in Lico-Net is constrained using infoNCE. In essence, the Lico-Net+D3C<sup>-</sup> can be interpreted as fixing the variance of the distributions established for all concepts in Lico-Net+D3C-cos to 0. The structure of Lico-Net+D3C<sup>-</sup> is illustrate in figure 19.

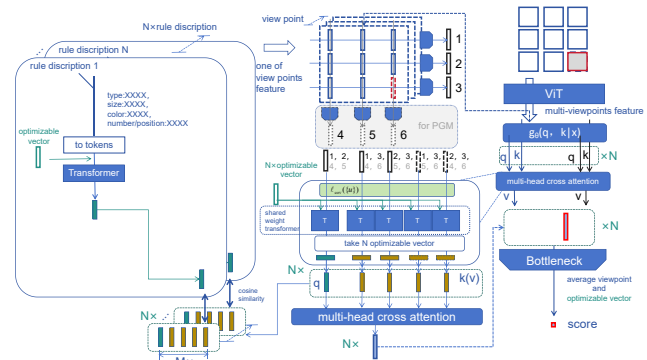


Fig. 19. Feedforward process of “Lico-Net+D3C<sup>-</sup>”

TABLE VI  
PROGRESSIVE PATTERN REASONING ACCURACIES AND OF MODELS ON PGM.

Model	Accuracy(%)		
	shape	line	answer
RS-Tran+Tranclip [28]	-	-	99.0
Meta Triple-CFN [32]	99.5	99.9	98.4
Meta Triple-CFN+Re-space layer [32]	99.7	99.9	99.3
Lico-Net+D3C <sup>-</sup>	99.7	99.9	99.3
Lico-Net+D3C	99.7	99.9	99.4
Lico-Net+D3C-cos	99.7	99.9	99.4

The D3C’s reasoning accuracys of progressive pattern are recorded in Table VI, highlighting the interpretability expressed by Lico-Net+D3C(-cos). It must be acknowledged that the experiment of applying D3C, which is based on the Sinkhorn distance, to Lico-Net was not conducted to its fullest extent in this paper. Once the experimental results of Lico-Net+D3C were sufficient to illustrate our point, we halted the model training. This was due to the significant computational resources required, even with the experimental equipment used in this paper: four A100s graphics cards. The training involved numerous epochs and tedious individual training epochs. This

was the intended purpose behind the design of D3C-cos as a replacement for D3C, as the power of Zeus needs to be conveyed by Hermes.

Despite achieving remarkable results in terms of reasoning accuracy and interpretability of progressive patterns with Lico-Net+D3C or D3C-cos, it is noteworthy that the improvement over previous works involving Meta data as additional auxiliary labels is not particularly striking. The possible reason for this is that the introduction of Meta data significantly reduces the difficulty of the RPM problem. Moreover, it is anticipated that a greater abundance of supervisory signals would correlate with enhanced intelligent performance.

However, Lico-Net+D3C still demonstrates distinct advantages that surpass other methods involving metadata. Specifically, Tranclip [28] utilizes metadata to pre-train a set of warm-start parameters for RS-Tran [28]. In other words, Tranclip fails to simultaneously endow RS-Tran with both interpretability of progressive patterns and high reasoning accuracy. Meta Triple-CFN [32] also relies on its specially designed Re-space Layer to enhance both its interpretability and reasoning accuracy. Similarly, the Re-Space Layer requires a fully trained Meta Triple-CFN to provide warm-start parameters [32]. In contrast, Lico-Net operates effectively without the necessity of a Re-space layer or a warm-start process, thereby simplifying the training procedure to a certain extent. This indicates that Lico-Net and D3C are more direct and effective, eliminating the need for indirect approaches. This "directness" reflects a more coherent and self-consistent logic of Lico-Net and D3C compared to other methods incorporating metadata.

This paper argues that this is not an insignificant contribution, as warm-start behavior may introduce unexpected instabilities, which are not a concern for Lico-Net and D3C. For example, when Tranclip [28] uses Meta data to produce warm-start parameters for RS-Tran, early stopping is required [28]. Neglecting this step may hinder Tranclip from improving or potentially worsen the reasoning performance of RS-Tran. The Re-space Layer [32] relies on a well-trained Meta Triple-CFN to provide warm-start parameters [32], a process that demands considerable training time and epochs. Inadequate training of these warm-start parameters can expose Meta Triple-CFN to risks akin to those faced by RS-Tran. The stopping timing for the preparation of both warm-start parameters requires manual determination and control, which brings numerous potential issues. In contrast, Lico-Net effectively mitigates these potential issues.

#### D. Ablation experiment on D2C and D4C

In the final of this section, we devised an experiment to validate the D2C and D4C approach. Utilizing a 500-step DDPM model, we generated a substantial quantity of Bongard-Logo data, specifically 3,180 Bongard-Logo images. According to the DDPM theory, these images belong to the same distribution as the real data, albeit with unknown semantics and concepts. During the training of ResNet50 and Triple-CFN, for each feedforward pass, we introduced 14 randomly selected DDPM-generated images as auxiliary group examples for the Bongard-Logo cases. The experimental results were recorded in "D2C<sup>-</sup>" item of the Table VII.

TABLE VII  
REASONING ACCURACIES OF MODELS ON BONGARD-LOGO.

Model	Accuracy(%)				
	Train	FF	BA	CM	NV
ResNet50 (infoNCE baseline)	92.0	88.9	98.0	76.1	76.0
Triple-CFN	93.2	92.0	98.2	78.0	78.1
ResNet50+D2C <sup>-</sup>	91.6	90.0	97.9	76.3	76.1
Triple-CFN+D2C <sup>-</sup>	93.0	92.1	98.2	77.9	78.2

It can be observed from the experiment results recorded in Table VII that introducing generated samples as negative examples is difficult to fundamentally alter the network's performance, as such behavior struggles to re-delineate the concepts. DDPM-generated data, sharing the same distribution as real data but with inherent uncertainties of concept and attribution, are limited in contributing to the delineation of concept boundaries.

D4C posits that the accuracy achieved by the discriminator in abstract reasoning problems is closely related to the quality of the positive and negative examples set in the task. The established examples serve to delineate the concept boundaries for abstract reasoning challenges. D2C, while attempting to define new concept boundaries for such problems, represents an imperfect methodology. Conversely, D4C emerges as a relatively more comprehensive approach. This ablation experiment aims to verify that, within the context of Bongard-Logo problems, the provision of meaningless negative examples—examples that do not meaningfully contribute to defining the boundaries of reasoning tasks—fails to enhance the discriminator's effectiveness. This finding echoes similar observations made in the RAVEN dataset, reinforcing the significance and rationale behind the design of D4C. Furthermore, it reaffirms D4C's assertion regarding the importance of high-quality positive and negative examples in abstract reasoning tasks. It also provides indirect evidence that the approaches of D2C and D4C extend beyond merely introducing additional negative examples. Instead, they aim to introduce negative examples that better delineate the boundaries of the problem.

## IX. CONCLUSION

In summary, D3C advocates for representing concepts in abstract reasoning problems using distributions. It posits that, compared to vectors, distributions are better suited to capture the high-dimensionality, abstractness, and complexity inherent in human concepts, and experimental evidence underscores the superiority of this approach. Additionally, D2C presents a novel approach to tackling Bongard-Logo and RPM problems by resampling training data and introducing new loss function terms, effectively outlining new boundaries for solutions to these challenges. However, the extent to which these boundaries adapt to the specific problems remains uncertain.

D4C builds upon the principles of both D2C and D3C, exploring the roles of positive and negative examples in abstract reasoning problems from a perspective on distribution. Specifically, positive examples are utilized to depict the mean



for deep networks, while negative examples contribute to describing the variance. Based on this understanding, D4C employs an adversarial approach, pitting the generator against the discriminator in repeated challenges. The generator continually produces negative examples that push the boundaries of the problem, while the discriminator refines its skills through repeated defense. This iterative process not only enhances the discriminator’s ability to distinguish between positive and negative examples but also improves the generator’s capacity to generate more sophisticated negative examples. Ultimately, this adversarial framework promotes the evolution of both components, leading to more robust and reliable solutions in abstract reasoning tasks.

For future, the D4C method presents a novel approach for abstract reasoning problems and even other discriminative tasks. Its exploration of the identities of positive and negative examples may provide insights for the development of other works.

## REFERENCES

- [1] Deng, J., Dong, W., Socher, R., Li, L. J., Li, K., & Fei-Fei, L. Imagenet: A large-scale hierarchical image database. In *IEEE Conference on Computer Vision and Pattern Recognition*, 246-255 (2009).
- [2] Krizhevsky, A., Sutskever, I., & Hinton, G. E. Imagenet classification with deep convolutional neural networks. *Communications of the ACM*, 60(6), 84-90 (2017).
- [3] He, K., Zhang, X., Ren, S., & Sun, J. Deep Residual Learning for Image Recognition. In *IEEE Conference on Computer Vision and Pattern Recognition*, 770-778 (2016).
- [4] Vaswani, A. *et al.* Attention is All You Need. In *Advances in Neural Information Processing Systems*, (2017).
- [5] Devlin, J., Chang, M. W., Lee, K., & Toutanova, K. Bert: Pre-training of Deep Bidirectional Transformers for Language Understanding. Preprint at <https://arxiv.org/abs/1810.04805> (2018).
- [6] Brown, T. *et al.* Language Models are Few-shot Learners. In *Advances in Neural Information Processing Systems*, 1877-1901 (2020).
- [7] Goodfellow, I. *et al.* Generative adversarial networks. *Communications of the ACM*, 63(11), 139-144 (2020).
- [8] Kingma, D. P., & Welling, M. Auto-encoding variational bayes. Preprint at <https://arxiv.org/abs/1312.6114> (2014).
- [9] Ho, J., Jain, A., & Abbeel, P. Denoising diffusion probabilistic models. In *Advances in Neural Information Processing Systems*, 33, 6840-6851 (2020).
- [10] Antol, S., Agrawal, A., Lu, J., Mitchell, M., Batra, D., Zitnick, C. L., & Parikh, D. VQA: Visual question answering. In *IEEE International Conference on Computer Vision*, 2425-2433 (2015).
- [11] Johnson, J., Hariharan, B., Van Der Maaten, L., Fei-Fei, L., Lawrence Zitnick, C., & Girshick, R. Girshick. CLEVR: A Diagnostic Dataset for Compositional Language and Elementary Visual Reasoning. In *IEEE Conference on Computer Vision and Pattern Recognition*, 2901-2910 (2017).
- [12] Depeweg, S., Rothkopf, C. A., & Jäkel, F. Solving Bongard Problems with a Visual Language and Pragmatic Reasoning. Preprint at <https://arxiv.org/abs/1804.04452> (2018).
- [13] Nie, W., Yu, Z., Mao, L., Patel, A. B., Zhu, Y., & Anandkumar, A. Bongard-LOGO: A New Benchmark for Human-Level Concept Learning and Reasoning. In *Advances in Neural Information Processing Systems*, 16468-16480 (2020).
- [14] Raven J. C. Raven’s Progressive Matrices. (Western Psychological Services, (1938).
- [15] Zhang, C., Gao, F., Jia, B., Zhu, Y., & Zhu, S. C. Raven: A Dataset for Relational and Analogical Visual Reasoning. In *Proceedings of the IEEE/CVF Conference on Computer Vision and Pattern Recognition*, 5317-5327 (2019).
- [16] Barrett, D., Hill, F., Santoro, A., Morcos, A., & Lillicrap, T. Measuring Abstract Reasoning in Neural Networks. In *International Conference on Machine Learning*, 511-520 (2018).
- [17] Dosovitskiy, A. *et al.* An Image is Worth 16x16 Words: Transformers for Image Recognition at Scale. Preprint at <https://arxiv.org/abs/2010.11929> (2020).
- [18] Zheng, K., Zha, Z. J., & Wei, W. Abstract Reasoning with Distracting Features. In *Advances in Neural Information Processing Systems*, (2019).
- [19] Zhang, C., Jia, B., Gao, F., Zhu, Y., Lu, H., & Zhu, S. C. Learning Perceptual Inference by Contrasting. In *Proceedings of Advances in Neural Information Processing Systems*, (2019).
- [20] Zhuo, T., & Kankanhalli, M. Effective Abstract Reasoning with Dual-Contrast Network. In *Proceedings of International Conference on Learning Representations*, (2020).
- [21] Benny, Y., Pekar, N., & Wolf, L. Scale-Localized Abstract Reasoning. In *Proceedings of the IEEE/CVF Conference on Computer Vision and Pattern Recognition*, 12557-12565, (2021).
- [22] Zhuo, Tao and Huang, Qiang & Kankanhalli, Mohan. Unsupervised abstract reasoning for raven’s problem matrices. *IEEE Transactions on Image Processing*, 8332-8341, (2021).
- [23] Wu, Y., Dong, H., Grosse, R., & Ba, J. The Scattering Compositional Learner: Discovering Objects, Attributes, Relationships in Analogical Reasoning. Preprint at <https://arxiv.org/abs/2007.04212> (2020).
- [24] Sahu, P., Basioti, K., & Pavlovic, V. SAVIR-T: Spatially Attentive Visual Reasoning with Transformers. Preprint at <https://arxiv.org/abs/2206.09265> (2022).
- [25] Zhang, C., Jia, B., Zhu, S. C., & Zhu, Y. Abstract Spatial-Temporal Reasoning via Probabilistic Abduction and Execution. In *Proceedings of the IEEE/CVF Conference on Computer Vision and Pattern Recognition*, 9736-9746 (2021).
- [26] Zhang, C., Xie, S., Jia, B., Wu, Y. N., Zhu, S. C., & Zhu, Y. Learning Algebraic Representation for Systematic Generalization. In *Proceedings of the European Conference on Computer Vision*, (2022).
- [27] Hersche, M., Zeqiri, M., Benini, L., Sebastian, A., & Rahimi, A. A Neuro-vector-symbolic Architecture for Solving Raven’s Progressive Matrices. Preprint at <https://arxiv.org/abs/2203.04571> (2022).
- [28] Q. Wei, D. Chen, B. Yuan, Multi-viewpoint and multi-evaluation with felicitous inductive bias boost machine abstract reasoning ability, *arXiv* :2210.14914, 2022.
- [29] Shi, Fan, Bin Li, and Xangyang Xue. "Abstracting Concept-Changing Rules for Solving Raven’s Progressive Matrix Problems." *arXiv preprint arXiv:2307.07734* (2023).
- [30] S.Kharagorgiev,"Solvingbongardproblemswithdeeplearning," [k10v.github.io,2020.](https://github.com/sk10v/solvingbongardproblemswithdeeplearning)
- [31] R.Song, B.Yuan. Solving the bongard-logo problem by modeling a probabilistic model. Preprint at <https://arxiv.org/abs/> arXiv:2403.03173 (2024).
- [32] R.Song, B.Yuan. Triple-CFN: Restructuring Concept Spaces for Enhancing Abstract Reasoning process. Preprint at <https://arxiv.org/abs/arXiv:2403.03190> (2024).
- [33] Shen, Jian, et al. "Wasserstein distance guided representation learning for domain adaptation." *Proceedings of the AAAI Conference on Artificial Intelligence*. Vol. 32. No. 1. 2018.
- [34] Cuturi, Marco. "Sinkhorn distances: Lightspeed computation of optimal transport." *Advances in neural information processing systems* 26 (2013).
- [35] Miyato, Takeru, et al. "Spectral normalization for generative adversarial networks." *arXiv preprint arXiv:1802.05957* (2018).
- [36] Arjovsky, Martin, Soumith Chintala, and Léon Bottou. "Wasserstein generative adversarial networks." *International conference on machine learning*. PMLR, 2017.
- [37] Hu, S., Ma, Y., Liu, X., Wei, Y., & Bai, S. Stratified Rule-Aware Network for Abstract Visual Reasoning. In *Proceedings of the AAAI Conference on Artificial Intelligence*, 1567-1574 (2021).
- [38] Zhuo, T., Huang, Q., & Kankanhalli, M. Unsupervised Abstract Reasoning for Raven’s Problem Matrices. *IEEE Transactions on Image Processing*, 8332 - 8341 (2021).
- [39] Carpenter, P. A., Just, M. A., & Shell, P. What One Intelligence Test Measures: a Theoretical Account of the Processing in the Raven Progressive Matrices Test. *Psychological review*, 97(3), 404, (1990).
- [40] Chen, T., Kornblith, S., Norouzi, M., & Hinton, G. A Simple Framework for Contrastive Learning of Visual Representations. In *Proceedings of the International Conference on Machine Learning*, 1597-1607 (2020).
- [41] Oord, A. V. D., Li, Y., & Vinyals, O. Representation Learning with Contrastive Predictive Coding. Preprint at <https://arxiv.org/abs/1807.03748> (2019).
- [42] He, K., Fan, H., Wu, Y., Xie, S., & Girshick, R. Momentum Contrast for Unsupervised Visual Representation Learning. In *Proceedings of the IEEE/CVF Conference on Computer Vision and Pattern Recognition*, 9729-9738 (2020).
- [43] Paszke, A. *et al.* Automatic Differentiation in Pytorch. In *NIPS Autodiff Workshop*, (2017).